JHEP

Published for SISSA by Springer

Received: July 30, 2019
Accepted: November 15, 2019
Published: December 9, 2019

Revisiting the new-physics interpretation of the $b \to c\tau\nu$ data

Rui-Xiang Shi,[a] **Li-Sheng Geng,**[a,b,c] **Benjamín Grinstein,**[d] **Sebastian Jäger**[e] **and Jorge Martin Camalich**[f,g]

[a] *School of Physics and Nuclear Energy Engineering, Beihang University, Beijing 100191, China*
[b] *International Research Center for Nuclei and Particles in the Cosmos, Beihang University, Beijing 100191, China*
[c] *Beijing Key Laboratory of Advanced Nuclear Materials and Physics, Beihang University, Beijing 100191, China*
[d] *Department of Physics, University of California, San Diego, 9500 Gilman Drive, La Jolla, CA 92093-0319, U.S.A.*
[e] *Department of Physics and Astronomy, University of Sussex, Brighton BN1 9QH, U.K.*
[f] *Instituto de Astrofísica de Canarias, C/Vía Láctea, s/n E38205, La Laguna, Tenerife, Spain*
[g] *Universidad de La Laguna, Departamento de Astrofísica, La Laguna, Tenerife, Spain*

E-mail: ruixiang.shi@buaa.edu.cn, lisheng.geng@buaa.edu.cn, bgrinstein@ucsd.edu, s.jaeger@sussex.ac.uk, jcamalich@iac.es

Abstract: We revisit the status of the new-physics interpretations of the anomalies in semileptonic B decays in light of the new data reported by Belle on the lepton-universality ratios $R_{D^{(*)}}$ using the semileptonic tag and on the longitudinal polarization of the D^* in $B \to D^*\tau\nu$, $F_L^{D^*}$. The preferred solutions involve new left-handed currents or tensor contributions. Interpretations with pure right-handed currents are disfavored by the LHC data, while pure scalar models are disfavored by the upper limits derived either from the LHC or from the B_c lifetime. The observable $F_L^{D^*}$ also gives an important constraint leading to the exclusion of large regions of parameter space. Finally, we investigate the sensitivity of different observables to the various scenarios and conclude that a measurement of the tau polarization in the decay mode $B \to D\tau\nu$ would effectively discriminate among them.

Keywords: Beyond Standard Model, Heavy Quark Physics

ArXiv ePrint: 1905.08498

https://doi.org/10.1007/JHEP12(2019)065

JHEP12(2019)065

Contents

1 Introduction

For some time now, the ratios of semileptonic B-decay rates,

$$R_{D^{(*)}} = \frac{\mathrm{BR}(B \to D^{(*)}\tau\nu)}{\mathrm{BR}(B \to D^{(*)}\ell\nu)} \qquad (\text{with } \ell = e \text{ or } \mu), \tag{1.1}$$

have appeared to be enhanced with respect to the Standard Model (SM) predictions with a global significance above the evidence threshold [1–11]. In addition, LHCb reports a value of the ratio

$$R_{J/\psi} = \frac{\mathrm{BR}(B_c^+ \to J/\psi\tau^+\nu_\tau)}{\mathrm{BR}(B_c^+ \to J/\psi\mu^+\nu_\mu)}, \tag{1.2}$$

about 2σ above the SM [10].

In the SM, semileptonic decays proceed via the tree-level exchange of a $W^\pm$ boson, preserving lepton universality. Hence, a putative NP contribution explaining the data must involve new interactions violating lepton universality. This may entail the tree-level exchange of new colorless vector (W') [12–17] or scalar (Higgs) [18–23] particles, or leptoquarks [24–49] with masses accessible to direct searches at the LHC.

Belle has also measured the longitudinal polarization of the τ ($P_\tau^{D^*}$) [6] and of the D^* ($F_L^{D^*}$) [50] in the $B \to D^*\tau\nu$ decay,

$$\begin{aligned} P_\tau^{D^*} &= \frac{\Gamma(\lambda_\tau = \frac{1}{2}) - \Gamma(\lambda_\tau = -\frac{1}{2})}{\Gamma(\lambda_\tau = \frac{1}{2}) + \Gamma(\lambda_\tau = -\frac{1}{2})}, \\ F_L^{D^*} &= \frac{\Gamma(\lambda_{D^*} = 0)}{\Gamma(\lambda_{D^*} = 1) + \Gamma(\lambda_{D^*} = 0) + \Gamma(\lambda_{D^*} = -1)}, \end{aligned} \tag{1.3}$$

JHEP12(2019)065

Observables	Data (averages)		SM
	HFLAV 2018	HFLAV 2019	
R_D	0.407(39)(24) corr $= -0.20$	0.340(27)(13) corr $= -0.38$	0.312(19)
R_{D^*}	0.306(13)(7)	0.295(11)(8)	0.253(4)
$R_{J/\psi}$	0.71(17)(18)		0.248(3)
$P_\tau^{D^*}$	$-0.38(51)(19)$		$-0.505(23)$
$F_L^{D^*}$	0.60(8)(4)		0.455(9)

Table 1. Data (averages) and predictions in the SM for semileptonic b-decay observables defined in eqs. (1.1)–(1.3). The Heavy Flavor Averaging Group (HFLAV) 2018 averages [65] of experimental data for R_D and R_{D^*} use data from BABAR [1, 2], Belle [3, 4, 6] and LHCb [5, 8, 9], while the HFLAV 2019 average includes the Belle measurement of both, R_D and R_{D^*}, with the semileptonic tag [51]. The LHCb measurement of $R_{J/\Psi}$ is reported in ref. [10] and the Belle measurements of $P_\tau^{D^*}$ and $F_L^{D^*}$ in refs. [10, 50]. The two experimental errors correspond to statistical and systematic uncertainties, respectively. SM predictions are obtained as specified in section 2.3.

where λ_X refers to the helicity of the particle X. While $P_\tau^{D^*}$ is reconstructed from the hadronic decays of the τ and is still statistically limited, the reported measurement of $F_L^{D^*}$ is rather precise and disagrees with the SM prediction with a significance of 1.7σ.

Recently, Belle announced a new combined measurement of both R_D and R_{D^*} using semileptonic decays for tagging the B meson in the event [51]. This presents a significant addition to the data set because the previous combined measurements of $R_{D^{(*)}}$ had been performed at the B factories using a hadronic tag. The new result is more consistent with the SM than the previous HFLAV average. Thus, these new data call for a reassessment of the significance of the tension of the signal with the SM and of the possible NP scenarios aiming at explaining it. The purpose of this work is to provide such an analysis using effective field theory (EFT) [52–63] and to relate it to (partial) UV completions in terms of simplified mediators. We assume that the lepton non-universal contribution affects only the couplings to the tau leptons. A comprehensive analysis of bounds on NP affecting $b \to c\ell\nu$ transitions can be found in ref. [64]. A summary of the recent data (averages) is shown in table 1, which is compared to the SM predictions which are obtained as specified in section 2.3.

2 Theoretical framework

2.1 Low-energy effective Lagrangian

The most general effective Lagrangian describing the contributions of heavy NP to semi-tauonic $b \to c\tau\bar{\nu}$ processes can be written as

$$\begin{aligned}\mathcal{L}_{\text{eff}}^{\text{LE}} \supset -\frac{4G_F V_{cb}}{\sqrt{2}}[&(1+\epsilon_L^\tau)(\bar{\tau}\gamma_\mu P_L \nu_\tau)(\bar{c}\gamma^\mu P_L b) + \epsilon_R^\tau(\bar{\tau}\gamma_\mu P_L \nu_\tau)(\bar{c}\gamma^\mu P_R b) \\ &+\epsilon_{S_L}^\tau(\bar{\tau}P_L \nu_\tau)(\bar{c}P_L b) + \epsilon_{S_R}^\tau(\bar{\tau}P_L \nu_\tau)(\bar{c}P_R b) + \epsilon_T^\tau(\bar{\tau}\sigma_{\mu\nu}P_L \nu_\tau)(\bar{c}\sigma^{\mu\nu}P_L b)] + \text{H.c.},\end{aligned} \tag{2.1}$$

where G_F is the Fermi constant and V_{cb} is the Cabibbo-Kobayashi-Maskawa (CKM) matrix element. The five Wilson coefficients (WCs) ϵ_L^τ, ϵ_R^τ, ϵ_T^τ, $\epsilon_{S_L}^\tau$ and $\epsilon_{S_R}^\tau$ encapsulate the NP

JHEP12(2019)065

contributions, featuring the scaling $\epsilon_\Gamma^\tau \sim \mathcal{O}(v^2/\Lambda_{\rm NP}^2)$, where $v \approx 246\,\text{GeV}$ is the electroweak symmetry breaking (EWSB) scale. In the context of the EFT of the SM (SMEFT) [66, 67], $\epsilon_R^\tau = \epsilon_R^\ell + \mathcal{O}(v^4/\Lambda_{\rm NP}^4)$ and the right-handed operator cannot contribute to lepton universality violation at leading order in the $(v^2/\Lambda_{\rm NP}^2)$ expansion [25, 68, 69]. For this reason, we do not consider the effect of ϵ_R^τ in our fits. Nonetheless, it is important to note that this assumption could be relaxed if there was not a mass gap between the NP and the EWSB scales, or under a nonlinear realization of the electroweak symmetry breaking [70].

The chirally-flipping scalar and tensor operators are renormalized by QCD and electroweak corrections [71–74]. The latter induce a large mixing of the tensor operator into $\epsilon_{S_L}^\tau$ which can have relevant implications for tensor scenarios [71]. As an illustration, defining $\vec{\epsilon}^{\,T}(\mu) = (\epsilon_{S_R}^\tau, \epsilon_{S_L}^\tau, \epsilon_T^\tau)(\mu)$, (where we have omitted flavor indices), we find that $\vec{\epsilon}\,(m_b) = M\ \vec{\epsilon}\,(1\ \text{TeV})$, with [71]

$$M = \begin{pmatrix} 1.737 & 0 & 0 \\ 0 & 1.752 & -0.287 \\ 0 & -0.0033 & 0.842 \end{pmatrix}, \tag{2.2}$$

and where, in a slight abuse of notation, we keep the notation for the WCs of the low-energy EFT above the EWSB scale. Operators with vector currents do not get renormalized by QCD, whereas electromagnetic and electroweak corrections produce a correction of a few percent to the tree-level contributions [71, 75]. On the other hand, all the operators in the SMEFT matching at low-energies to the Lagrangian in eq. (2.1) can give, under certain assumptions on the flavor structure of the underlying NP, large contributions to other processes such as decays of electroweak bosons, the τ lepton and the Higgs, or the anomalous magnetic moment of the muon [74, 76, 77].

An interesting scenario where the new physics cannot be described by the local effective Lagrangian eq. (2.1) consists of the addition of new light right-handed neutrinos [13, 15–17, 32, 78, 79]. This duplicates the operator basis given in eq. (2.1) by the replacements $P_L \to P_R$ in the leptonic currents (and in the hadronic current for the tensor operator) [69, 78, 80] and whose WCs we label with $\epsilon_\Gamma \to \tilde{\epsilon}_\Gamma$. None of these operators interfere with the SM and their contributions to the decay rates are, thus, quadratic and positive. This also means that the size of the NP contributions needed to explain $R_{D^{(*)}}$ in this case are larger than with the operators in eq. (2.1) and they typically enter in conflict with bounds from other processes like the decay $B_c \to \tau\nu$ [81, 82] or from direct searches at the LHC [83]. As an illustration of the features and challenges faced by these models we consider the operator with right-handed currents,

$$\mathcal{L}_{\rm eff}^{\rm LE} \supset -\frac{4G_F V_{cb}}{\sqrt{2}} (\tilde{\epsilon}_R^\tau \bar{\tau}\gamma_\mu N_R)(\bar{c}\gamma^\mu P_R b) + \text{H.c.}, \tag{2.3}$$

(with N_R denoting the right-handed neutrino), which incarnates a popular NP interpretation of the anomaly [13, 15–17, 78, 79]. Finally, imaginary parts also contribute quadratically to the rates so we assume the WCs to be real, although we will briefly study also the impact of imaginary parts below.

JHEP12(2019)065

Mediator	Spin	SU(3)	SU(2)	U(1)	ϵ_L^τ	$\tilde{\epsilon}_R^\tau$	$\epsilon_{S_R}^\tau$	$\epsilon_{S_L}^\tau$	ϵ_T^τ
H	0	**1**	**2**	$+1/2$	✗	✗	✓	✓	✗
W'_L	1	**1**	**3**	0	✓	✗	✗	✗	✗
W'_R	1	**1**	**1**	$+1$	✗	✓	✗	✗	✗
S_1	0	$\overline{\mathbf{3}}$	**1**	$+1/3$	✓	✓	✗	✓	✓
S_3	0	$\overline{\mathbf{3}}$	**3**	$+1/3$	✓	✓	✗	✗	✗
R_2	0	**3**	**2**	$+7/6$	✓	✓	✗	✓	✓
U_1	1	**3**	**1**	$+2/3$	✓	✓	✓	✗	✗
U_3	1	**3**	**3**	$+2/3$	✓	✓	✗	✗	✗
V_2	1	$\overline{\mathbf{3}}$	**2**	$+5/6$	✗	✗	✓	✗	✗

Table 2. Quantum numbers of mediators that can explain at tree-level the $R_{D^{(*)}}$ anomalies and their contributions to the effective operators in eqs. (2.1), (2.3).

2.2 Simplified models

The effective operators in eqs. (2.1), (2.3) can be mediated at tree level by a number of new particles, that we list in table 2. Possibilities with new charged colorless weak bosons can be realized with the W' in either a triplet (W'_L) or a singlet (W'_R) representation of weak isospin. In the former case, the neutral component of the triplet, a Z' with a mass close to the one of the W', produces large effects in either neutral-meson mixing or di-tau production at the LHC, so that this scenario is unavoidably in conflict with data [84]. Making the W' a singlet of weak isospin, W'_R=(**1**, **1**,+1) under SU(3) × SU(2) × U(1), requires introducing right-handed neutrinos to contribute to $b \to c\tau\bar{\nu}$ [13, 15–17]; parametrizing the Lagrangian for this model,

$$\mathcal{L}_{W'} \supset \left(g_{cb}\bar{c}\gamma_\mu P_R b + g_{\tau N}\bar{N}_R\gamma_\mu P_R\tau\right) W'^{\mu}_R + \text{h.c.}, \tag{2.4}$$

one finds the contribution to the EFT,

$$V_{cb}\tilde{\epsilon}_R^\tau = \frac{g_{cb}g^*_{\tau N}}{2}\frac{v^2}{m^2_{W'}}. \tag{2.5}$$

Models based on extending the scalar sector of the SM, such as the two-Higgs doublet model (labeled by H in table 2), generate the scalar operators through charged-Higgs exchange. However, these are disfavored by experimental bounds that stem from the B_c lifetime [81] and from the branching fraction of $B_c \to \tau\nu$ derived using LEP data [82]. Strong limits from direct searches at the LHC of the corresponding charged scalars have also been obtained in the literature [85].

On the other hand, leptoquark exchanges can produce all the operators in eq. (2.1).[1] The SM interactions of the scalar leptoquark S_1=($\overline{\mathbf{3}}$, **1**,+1/3) can be described by the Lagrangian,

$$\mathcal{L}_{S_1} \supset y^{LL}_{1,i\alpha}\bar{Q}^c_{L,i}\,\epsilon\, L_{L,\alpha}S_1 + y^{RR}_{1,i\alpha}\bar{u}^c_{R,i}\, e_{R,\alpha}S_1 + y^{\overline{RR}}_{1,i\alpha}\bar{d}^c_{R,i}\, N_{R,\alpha}S_1, \tag{2.6}$$

[1] We follow the notation to label the leptoquark fields introduced in refs. [86, 87].

JHEP12(2019)065

where ϵ_{ab} is the antisymmetric tensor of rank two and where we are labeling the flavor of the fields in the interaction basis. This model produces left-handed, scalar-tensor and right-handed contributions [24, 29, 33, 34],

$$V_{cb}\epsilon_L^\tau = \frac{\tilde{y}^{LL,d}_{1,33}(\tilde{y}^{LL,u}_{1,23})^*}{4}\frac{v^2}{m^2_{S_1}}, \qquad V_{cb}\epsilon^\tau_{S_L} = -4V_{cb}\epsilon^\tau_T = \frac{\tilde{y}^{LL,d}_{1,33}(\tilde{y}^{RR}_{1,23})^*}{4}\frac{v^2}{m^2_{S_1}},$$
$$V_{cb}\tilde{\epsilon}_R^\tau = -\frac{\tilde{y}^{\overline{RR}}_{1,33}(\tilde{y}^{RR}_{1,23})^*}{4}\frac{v^2}{m^2_{S_1}}, \tag{2.7}$$

where the coefficients are defined at a scale equal to the leptoquark mass, $\mu = m_{S_1}$. The tilde in the coefficients of eq. (2.7) and in the rest of this subsection indicates that the quark unitary rotations have been absorbed in the definition of the couplings. For instance, if such transformations are $d_L \to L_d\ d_L$, $u_L \to L_u\ u_L$, $d_R \to R_d\ d_R$, $u_R \to R_u\ u_R$, we have defined $\tilde{y}^{LL,u(d)}_{1,i\alpha} = [y_1^{LL}\ L_{u(d)}]_{i\alpha}$, $\tilde{y}^{RR}_{1,i\alpha} = [y_1^{RR}\ R_u]_{i\alpha}$ and $\tilde{y}^{\overline{RR}}_{1,i\alpha} = [y_1^{\overline{RR}}\ R_d]_{i\alpha}$ where summation of quark flavor indices is implicit. We have also defined these couplings in the charged-lepton mass basis, ignoring neutrino masses.

The leptoquark with quantum numbers R_2=($\mathbf{3}$, $\mathbf{2}$,+7/6) and Lagrangian,

$$\mathcal{L}_{R_2} \supset -y^{RL}_{2,i\alpha}\bar{u}_{R,i}\ \epsilon\ L_{L,\alpha}R_2 + y^{LR}_{2,i\alpha}\bar{Q}_{L,i}e_{R,\alpha}R_2, \tag{2.8}$$

leads to

$$V_{cb}\epsilon^\tau_{S_L} = +4V_{cb}\epsilon^\tau_T = \frac{\tilde{y}^{RL}_{2,23}(\tilde{y}^{LR,d}_{2,33})^*}{4}\frac{v^2}{m^2_{R_2}}. \tag{2.9}$$

Thus, one can achieve a tensor scenario by adjusting the masses and couplings of the S_1 and R_2 leptoquarks. It is important to stress that such a solution at low energies requires some tuning due to the large electroweak mixing into scalar operators in eq. (2.2).

Among the vector leptoquarks we consider the U_1=($\mathbf{3}$, $\mathbf{1}$,+2/3), which has been extensively studied in the interpretation of the B anomalies [25, 26, 35–37, 39–42, 44, 46–48],

$$\mathcal{L}_{U_1} \supset \chi^{LL}_{1,i\alpha}\bar{Q}_{L,i}\gamma_\mu L_{L,\alpha}U_1^\mu + \chi^{RR}_{1,\alpha}\bar{d}_{R,i}\gamma_\mu e_{R,\alpha}U_1^\mu + \chi^{\overline{RR}}_{1,i\alpha}\bar{u}_{R,i}\gamma_\mu N_{R,\alpha}U_1^\mu, \tag{2.10}$$

leading to left-handed and right-handed contributions, and a scalar contribution,

$$V_{cb}\epsilon_L^\tau = \frac{\tilde{\chi}^{LL,u}_{1,23}(\tilde{\chi}^{LL,d}_{1,33})^*}{2}\frac{v^2}{m^2_{U_1}}, \qquad V_{cb}\tilde{\epsilon}_R^\tau = \frac{\tilde{\chi}^{\overline{RR}}_{1,23}(\tilde{\chi}^{RR}_{1,33})^*}{2}\frac{v^2}{m^2_{U_1}},$$
$$V_{cb}\epsilon^\tau_{S_R} = -\tilde{\chi}^{LL,u}_{1,23}(\chi^{\overline{RR}}_{1,33})^*\frac{v^2}{m^2_{U_1}}. \tag{2.11}$$

In particular, a combination of left-handed and right-handed couplings gives rise to a scalar operator which is instrumental to achieve a better agreement with data in some UV completions of the U_1 leptoquark [37, 42, 47, 48].

The mediators S_3=($\overline{\mathbf{3}}$, $\mathbf{3}$,+1/3) and U_3=($\overline{\mathbf{3}}$, $\mathbf{3}$,+2/3) in table 2 provide completions of the left-handed current operator equivalent to the S_1 and U_1 ones for scalar and vector leptoquark scenarios, respectively. Finally, we have not included in the table the leptoquarks $\tilde{R}_2 = (\mathbf{3}, \mathbf{2}, +1/6)$ and $\tilde{V}_2 = (\overline{\mathbf{3}}, \mathbf{2}, -1/6)$ because they only contribute to scalar and tensor operators with right-handed neutrinos which are not considered in this work, as argued in section 2.1.

JHEP12(2019)065

2.3 Form factors

The hadronic matrix elements in the $b \to c$ decay amplitudes are parameterized in terms of the following form factors,

$$
\begin{aligned}
\langle D(k)|\bar{c}\gamma^\mu b|\bar{B}(p)\rangle &= (p+k)^\mu f_+(q^2) + (p-k)^\mu \frac{m_B^2 - m_D^2}{q^2}(f_0(q^2) - f_+(q^2)),\\
\langle D(k)|\bar{c}b|\bar{B}(p)\rangle &= \frac{m_B^2 - m_D^2}{m_b - m_c} f_0(q^2),\\
\langle D(k)|\bar{c}\sigma^{\mu\nu}b|\bar{B}(p)\rangle &= \frac{2i f_T(q^2)}{m_B + m_D}(k^\mu p^\nu - p^\mu k^\nu),\\
\langle D(k)|\bar{c}\sigma^{\mu\nu}\gamma_5 b|\bar{B}(p)\rangle &= \frac{2 f_T(q^2)}{m_B + m_D}\epsilon^{\mu\nu\alpha\beta}k_\alpha p_\beta,\\
\langle V(k,\epsilon)|\bar{c}\gamma^\mu b|P(p)\rangle &= \frac{2iV(q^2)}{m_P + m_V}\epsilon^{\mu\nu\alpha\beta}\epsilon^*_\nu k_\alpha p_\beta,\\
\langle V(k,\epsilon)|\bar{c}\gamma_5 b|P(p)\rangle &= -\frac{2m_V}{m_b + m_c}A_0(q^2)\epsilon^*\cdot q,\\
\langle V(k,\epsilon)|\bar{c}\gamma^\mu\gamma_5 b|P(p)\rangle &= 2m_V A_0(q^2)\frac{\epsilon^*\cdot q}{q^2}q^\mu + (m_P + m_V)A_1(q^2)\left(\epsilon^{*\mu} - \frac{\epsilon^*\cdot q}{q^2}q^\mu\right)\\
&\quad - A_2(q^2)\frac{\epsilon^*\cdot q}{m_P + m_V}\left((p+k)^\mu - \frac{m_P^2 - m_V^2}{q^2}q^\mu\right)\\
\langle V(k,\epsilon)|\bar{c}\sigma^{\mu\nu}b|P(p)\rangle &= \frac{\epsilon^*\cdot q}{(m_P + m_V)^2}T_0(q^2)\epsilon^{\mu\nu\alpha\beta}p_\alpha k_\beta\\
&\quad + T_1(q^2)\epsilon^{\mu\nu\alpha\beta}p_\alpha\epsilon^*_\beta + T_2(q^2)\epsilon^{\mu\nu\alpha\beta}k_\alpha\epsilon^*_\beta,\\
\langle V(k,\epsilon)|\bar{c}\sigma^{\mu\nu}\gamma_5 b|P(p)\rangle &= \frac{i\epsilon^*\cdot q}{(m_P + m_V)^2}T_0(q^2)(p^\mu k^\nu - k^\mu p^\nu)\\
&\quad + iT_1(q^2)(p^\mu\epsilon^{*\nu} - \epsilon^{*\mu}p^\nu) + iT_2(q^2)(k^\mu\epsilon^{*\nu} - \epsilon^{*\mu}k^\nu),
\end{aligned}
\tag{2.12}
$$

where $q = p - k$, $\epsilon_{0123} = 1$, V and P stand for vector mesons (D^* and J/ψ) and pseudoscalar mesons (B and B_c), respectively. We take the quark masses in the $\overline{\rm MS}$ scheme, i.e, $m_b \equiv \overline{m}_b(\overline{m}_b) = 4.18\,\text{GeV}$ and $\overline{m}_c(\overline{m}_c) = 1.27\,\text{GeV}$ [88]. Note that the c-quark mass is derived by the solution of the renormalization group equation for $\overline{m}_c(\mu)$ at two-loop order and $\alpha_s(\mu)$ with three-loop accuracy [89]. We follow the PDG [88] for the masses of the mesons relevant in this work.

For the $B \to D^{(*)}$ mode, some of the form factors are taken from Lattice QCD calculations [90, 91]. The rest are parameterized using heavy-quark effective theory (HQET) [92–99] whose nuisance parameters are determined by the HFLAV global fits to the $\bar{B} \to D^{(*)}\ell^-\bar{\nu}$ data [100]. Our determination of R_D and R_{D^*} differs from that of HFLAV in the choice of form factors; ours, based on ref. [101], do not include some recent refinements [102–104].

For the $B_c \to J/\psi$ form factors, they have been studied in a variety of approaches [105–115] (for earlier analysis focused on this decay mode see refs. [115–118]). Here we take $V(q^2)$, $A_0(q^2)$, $A_1(q^2)$ and $A_2(q^2)$ calculated in the covariant light-front quark model [110]

JHEP12(2019)065

because these results are well consistent with the lattice results at all available q^2 points in refs. [113, 114]. The three tensor form factors can be related through the corresponding HQET form factor $h_{A_1}(\omega)$ at leading order in the heavy-quark expansion,

$$\begin{aligned} A_1(\omega) &= (\omega+1)\frac{\sqrt{m_{B_c} m_{J/\psi}}}{m_{B_c}+m_{J/\psi}} h_{A_1}(\omega), & T_0(\omega) &= \mathcal{O}(\Lambda/m_Q), \\ T_1(\omega) &= \sqrt{m_{J/\psi}/m_{B_c}}\, h_{A_1}(\omega) + \mathcal{O}(\Lambda/m_Q), & T_2(\omega) &= \sqrt{m_{B_c}/m_{J/\psi}}\, h_{A_1}(\omega) + \mathcal{O}(\Lambda/m_Q), \end{aligned} \tag{2.13}$$

with $\omega = v_{J/\psi} \cdot v_{B_c} = (m_{B_c}^2 + m_{J/\psi}^2 - q^2)/(2 m_{B_c} m_{J/\psi})$ and where we have neglected the Λ/m_Q power corrections.

2.4 Statistical method

We follow a frequentist statistical approach to compare the measured values of $n_{\rm exp}$ observables, $\vec{O}^{\rm exp}$, to their theoretical predictions $\vec{O}^{\rm th}$ as functions of the Wilson coefficients $\vec{\epsilon}$, and of nuisance theoretical parameters $\vec{y}$. The nuisance parameters parameterize the lack of knowledge (theoretical uncertainties) of the form factors. For the $B \to D^{(*)}$ decays, we employ the parametrization and numerical inputs (including correlations) described in ref. [101]. For the $B_c \to J/\Psi$ decays we parameterize the theoretical errors reported for the form factors in ref. [110] as uncorrelated nuisance parameters. We then define a test statistic

$$\tilde{\chi}^2(\vec{\epsilon},\ \vec{y}) = \chi^2_{\rm exp}(\vec{\epsilon},\ \vec{y}) + \chi^2_{\rm th}(\vec{y}), \tag{2.14}$$

where

$$\begin{aligned} \chi^2_{\rm exp}(\vec{\epsilon},\ \vec{y}) &= [\vec{O}^{\ \rm th}(\vec{\epsilon},\ \vec{y}) - \vec{O}^{\ \rm exp}]^T \cdot (V^{\rm exp})^{-1} \cdot [\vec{O}^{\ \rm th}(\vec{\epsilon},\ \vec{y}) - \vec{O}^{\ \rm exp}], \\ \chi^2_{\rm th}(\vec{y}) &= (\vec{y} - \vec{y}_0)^T \cdot (V^{\rm th})^{-1} \cdot (\vec{y} - \vec{y}_0), \end{aligned} \tag{2.15}$$

$\vec{y}_0$ are a set of central values for the nuisance parameters, and $V^{\rm exp}$ and $V^{\rm th}$ denote the experimental and theoretical covariance matrices, respectively. By adding the theory term $\chi^2_{\rm th}$ we have in effect (from a statistical point of view) added $n_{\rm th}$ (correlated) "measurements" of the $n_{\rm th}$ theory parameters to the $n_{\rm exp}$ measurements of the observables.

We will consider scenarios (statistical models) with different subsets of the Wilson coefficients allowed to vary and the remaining ones set to zero, and with various subsets of the experimental observables included. In each case, we obtain best-fit values for the model parameters, including the nuisance parameters, by minimizing χ^2. To do so, in a first step we construct a profile-χ^2 function

$$\chi^2(\vec{\epsilon}) = \min_{\vec{y}} \tilde{\chi}^2(\vec{\epsilon},\ \vec{y}), \tag{2.16}$$

which depends solely on the subset of Wilson coefficients allowed to take nonzero values in a particular scenario, which we again refer to as $\vec{\epsilon}$. (Note that in the case of a single measurement of an observable whose theoretical expression depends linearly on a single

theory nuisance parameter y, such that $y-y_0$ is proportional to the theoretical uncertainty, the profiling reproduces the widely employed prescription of combining theoretical and experimental errors in quadrature.) In a second step, we minimize $\chi^2(\vec{\epsilon})$ over $\vec{\epsilon}$; the value(s) of $\vec{\epsilon}$ at the minimum χ^2_{min} provide(s) the best fit (maximum likelihood fit).

Next, we compute a p-value to quantify the goodness of fit, i.e. how well a given scenario can describe the data. We will assume that $\chi^2(\vec{\epsilon})$ follows a χ^2-distribution with $n_{\text{dof}} = n_{\text{exp}} - n_\epsilon$ degrees of freedom, where n_ϵ is the number of parameters allowed to vary in a given fit. Note that the theory parameters do not contribute to n_{dof} because χ^2_{th} contains as many "measurements" as theory parameters. In each scenario, the p-value is obtained from χ^2_{min} as one minus the cumulative χ^2 distribution for n_{dof} degrees of freedom. To illustrate this, let us consider only the χ^2_{exp} including R_D and R_{D*} and ask how well the SM describes these data. For simplicity, let us neglect theory errors altogether (they will be included in the following section, with little impact on the result), taking the SM prediction to be the central values employed by HFLAV2019, $R_D^{\text{SM,HFLAV}} = 0.299$ and $R_{D^*}^{\text{SM,HFLAV}} = 0.258$. In this case, there are no parameters to minimize over and χ^2 is simply a number. This is easily obtained from the HFLAV2019 averages and correlation shown in table 1, substituting the SM values for the observables, which gives $\Delta\chi^2_{\text{SM}} = \Delta\chi^2(\vec{0})$ as defined below, and adding a constant $\chi^2_{\text{min}} = 8.7$ as stated by HFLAV.[2] Nine measurements entered the combination and we are determining zero parameters, resulting in $n_{\text{dof}} = 9$. With $\chi^2_{\text{SM}} = \chi^2(\vec{\epsilon} = \vec{0}) = 22.8$, this gives a p-value of 6.56×10^{-3} corresponding to 2.72σ, slightly reduced from 3.00σ obtained in an analogous manner from the HFLAV2018 combination.

Finally, for each one-parameter BSM scenario, we construct $\Delta\chi^2(\vec{\epsilon}) = \chi^2(\vec{\epsilon}) - \chi^2_{\text{min}}$ and obtain $n\sigma$ confidence intervals from the requirement $\Delta\chi^2 \leq n^2$. Similarly, for each 2-parameter scenario we construct the corresponding $\Delta\chi^2$ and obtain two-dimensional 1σ and 2σ regions from the conditions $\Delta\chi^2 \leq 2.3$ and $\Delta\chi^2 \leq 6.18$, respectively. We also determine, for each model,

$$\Delta\chi^2_{\text{SM}} = \chi^2(\vec{0}) - \chi^2_{\text{min}},$$

to quantify at what level the SM point is excluded in that model. The $\sqrt{\Delta\chi^2_{\text{SM}}}$ is converted to an equivalent number of standard deviations, referred to as the pull Pull_{SM}, by employing the cumulative χ^2-distribution with n_{dof} set to 1 or 2, the number of jointly determined parameters, as appropriate.

Let us close this section by contrasting to the usual approach for comparing the R_D and R_{D^*} measurements to the SM, as employed by HFLAV. In this approach, the true values of R_D and R_{D^*} are treated as free parameters, which effectively amounts to a two-parameter BSM model. In this model, HFLAV obtain an SM pull of 3.08σ. We stress that this is a statement about how much better than the SM a BSM model can potentially describe the data. It is conceptually analogous to the pulls in our two-parameter Wilson coefficient fits. (In fact, we will find in the next section a slightly higher pull for two of our 1-parameter models. This comes about because a given $\Delta\chi^2$ value implies a lower p-value (higher number of standard deviations) when determining a single parameter as opposed

[2] By adding χ^2_{min} we are taking into account the goodness of the HFLAV fit to the different measurements of $R_{D^{(*)}}$ which is needed to obtain an accurate estimate of the p-values.

JHEP12(2019)065

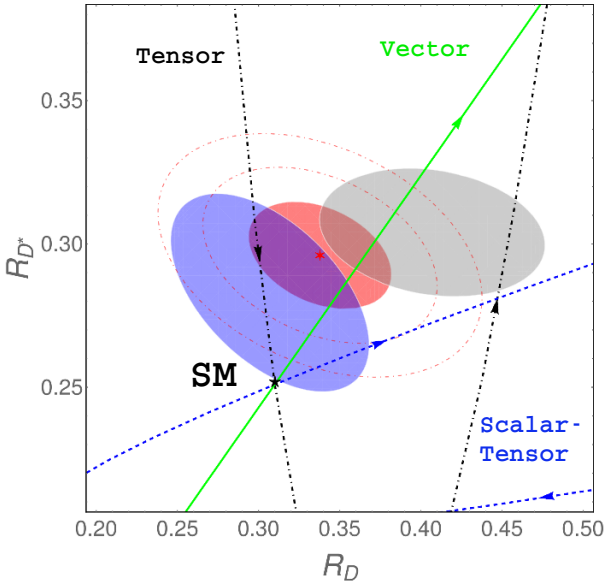

Figure 1. Trajectories in the $(R_D,\ R_{D^*})$ plane of predicted deviations from the SM due to NP where the arrows indicate the direction of positive increment of the WCs as defined in eq. 2.1. "Vector" corresponds to either ϵ_L^τ or $\tilde{\epsilon_R}^\tau$ while "tensor" and "scalar-tensor" correspond to ϵ_T^τ and $\epsilon_{S_L}^\tau = -4\epsilon_T^\tau$, respectively, at $\mu = 1\,\text{TeV}$ and evolved down to $\mu = m_b$ using eq. (2.2). The gray, blue and red solid ellipses are the 1σ contours of the 2018 HFLAV average, the Belle measurement with semileptonic tag, and of the combination of the two, respectively. Red dot-dashed ellipses are 2σ and 3σ contours of the combination.

to joint determination of two parameters.) Conversely, our SM p-values are a statement how well the SM describes the data, *without reference to any comparator BSM model*. As we have seen, the data is marginally consistent with the SM at 3σ, little changed from 2018. As we will see in the subsequent sections, the impact of the new Belle data on the best-fit values in BSM scenarios is much stronger.

3 Results

In this section, we investigate the values of the WCs determined by fitting to the experimental data of R_D, R_{D^*}, $R_{J/\psi}$, $P_\tau^{D^*}$ and $F_L^{D^*}$ given in table 1. We also discuss the constraints on scalar operators derived from the limits $\text{Br}(B_c \to \tau\nu) \leq 30\%(10\%)$ which are obtained using the B_c lifetime [81] (LEP searches of the decays $B_{(c)} \to \tau\nu$ [82]). Note that these limits have been critically discussed in refs. [58, 119, 120]. Finally, an upper bound on the values of the WCs can be derived from the tails of the monotau signature ($pp \to \tau_h X$+MET) at the LHC [83, 121, 122] (see below). We will perform fits to two types of dataset: $R_{D^{(*)}}$ only, as well as to the full dataset in table 1 including in addition $R_{J/\psi}$ and the polarization observables.

3.1 Fits to $R_{D^{(*)}}$ only

In figure 1 we show the "trajectories" representing the correlated impact on R_D and R_{D^*} of NP scenarios where only a single operator is present at a certain scale. Namely, the

JHEP12(2019)065

	Best fit	$\chi^2_{\rm min}$	p-value	$\text{Pull}_{\rm SM}$	1σ range
ϵ_L^τ	0.07	9.00	0.34	3.43	$(0.05, 0.09)$
ϵ_T^τ	-0.03	9.85	0.28	3.30	$(-0.04, -0.02)$
$\epsilon_{S_L}^\tau$	0.09	19.14	1.41×10^{-2}	1.27	$(0.02, 0.15)$
$\epsilon_{S_R}^\tau$	0.13	15.84	4.47×10^{-2}	2.22	$(0.07, 0.20)$
$\tilde{\epsilon}_R^\tau$	0.38	9.00	0.34	3.43	$(0.32, 0.44)$
$\epsilon_{S_L}^\tau = -4\epsilon_T^\tau$	0.09	12.25	0.14	2.92	$(0.06, 0.12)$
$(\epsilon_{S_L}^\tau, \epsilon_T^\tau)$	$(0.07, -0.03)$	8.7	0.27	3.03	$\epsilon_{S_L}^\tau \in (0.00, 0.14)$ $\epsilon_T^\tau \in (-0.04, -0.02)$
$(\epsilon_{S_L}^\tau, \epsilon_{S_R}^\tau)$	$(-0.47, 0.53)$	8.7	0.27	3.03	$\epsilon_{S_L}^\tau \in (-0.66, -0.30)$ $\epsilon_{S_R}^\tau \in (0.37, 0.69)$
$(\epsilon_{S_R}^\tau, \epsilon_T^\tau)$	$(0.07, -0.03)$	8.7	0.27	3.03	$\epsilon_{S_R}^\tau \in (0.00, 0.14)$ $\epsilon_T^\tau \in (-0.04, -0.02)$
$(\epsilon_L^\tau, \epsilon_T^\tau)$	$(0.05, -0.01)$	8.7	0.27	3.03	$\epsilon_L^\tau \in (0.00, 0.09)$ $\epsilon_T^\tau \in (-0.03, 0.01)$
$(\epsilon_L^\tau, \epsilon_{S_L}^\tau)$	$(0.08, -0.04)$	8.7	0.27	3.03	$\epsilon_L^\tau \in (0.05, 0.10)$ $\epsilon_{S_L}^\tau \in (-0.13, 0.04)$
$(\epsilon_L^\tau, \epsilon_{S_R}^\tau)$	$(0.08, -0.05)$	8.7	0.27	3.03	$\epsilon_L^\tau \in (0.05, 0.11)$ $\epsilon_{S_R}^\tau \in (-0.15, 0.04)$

Table 3. Best fit values, $\chi^2_{\rm min}$, p-value, pull and 1σ confidence intervals of the WCs in the fits to all the $R_{D^{(*)}}$ data. We perform fits to one or two WCs at a time with the understanding that the others are set to 0. For the cases of two Wilson-coefficient fits, the 1σ interval of each Wilson coefficient is obtained by profiling over the other one to take into account their correlation.

"vector" curve is followed by scenarios with new pure left-handed (ϵ_L^τ) or pure right-handed ($\tilde{\epsilon_R}^\tau$) currents (which are not affected by short distance QCD corrections). "Tensor" and "scalar-tensor" interpretations involve both ϵ_T^τ and $\epsilon_{S_L}^\tau$ coupled by the radiative corrections in the SM, cf. eq. (2.2). The tensor trajectory describes a solution with only the tensor operator produced at the heavy scale (cf. produced by the combination of S_1- and R_2-leptoquark contributions described in section 2.2), that we take to be 1 TeV. The scalar-tensor description assumes the relation $\epsilon_{S_L}^\tau(1\text{ TeV}) = -4\epsilon_T^\tau(1\text{ TeV})$, again, at the heavy scale (cf. produced by the S_1 leptoquark). The arrows in the curves signal the direction of positive increment of the WCs. The experimental data in table 1 is represented by the different ellipses: the gray one is the 1σ contour of the 2018 HFLAV average, the blue ellipse is the 1σ region of the 2019 Belle measurement with semi-leptonic tag and, finally, the red ellipses are the 1σ, 2σ and 3σ contours of the combination of these two.

The interference of the SM with left-handed or scalar-tensor contributions can produce a simultaneous increase of R_D and R_{D^*}, as illustrated in figure 1 by the positive slope of the corresponding curves at the SM point. This effect drives these solutions to agree well with the 2018 HFLAV average. In case of the tensor scenario, interference with the SM increases R_D at the expense of reducing R_{D^*} or vice versa. This effect is illustrated by the negative slope of the "Tensor" curve in figure 1. Therefore, the agreement of this scenario with the older data set is due to the quadratic contributions of the tensor operator to the rates. With the new Belle measurement, R_D becomes more consistent with the SM while a value of R_{D^*} larger than predicted is still favored. In this new scenario, "vector" models still agree with the data but now the interference of the tensor operator with the SM can play a role in providing a satisfactory solution.

In table 3 we show the results of fits to all the data on $R_{D^{(*)}}$ of one or two WCs at a time, while setting the others to zero. In the two-dimensional case we only investigate

JHEP12(2019)065

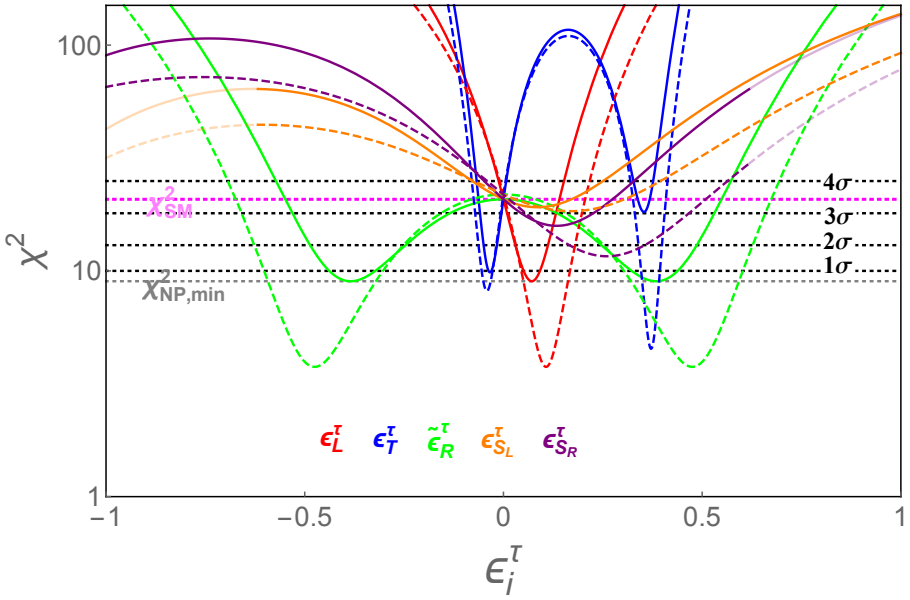

Figure 2. The χ^2 of the fits to R_D and R_{D^*} with one Wilson coefficient active at a time (setting the others to 0) and evaluated at the renormalization scale $\mu = m_b$. The solid lines correspond to the fits to the 2019 HFLAV average. Horizontal lines show the value at the minima of the model giving the best fit (vector scenario) and the 1σ to 4σ ranges computed from there. We also show the line corresponding to the value of $\chi^2_{\rm SM}$. The dashed lines correspond to the fits to the 2018 HFLAV average. Faded regions for $\epsilon^\tau_{S_L}$ and $\epsilon^\tau_{S_R}$ represent a exclusion of 30% limit on Br($B_c \to \tau\nu$).

the interplay between operators with left-handed neutrinos. Setting all WCs to zero, one obtains a $\chi^2_{\rm SM} = 20.75$. With 9 degrees of freedom (d.o.f.) this corresponds to a p-value of 1.38×10^{-2}. As can be inferred from the table, the "vector" operators provide the best one-parameter fit to the data, with a p-value of 0.34 and a SM pull of 3.43σ. The difference in size of the values of the WCs between the left- and right-handed vector solutions is due to the fact that the latter corresponds to a quadratic NP effect in the rates.

The tensor operator also gives a good fit to the data, where the solution driven by the interference piece is now preferred. Scalar models do not provide good fits and require values that may be in conflict with the bounds from $B_c \to \tau\nu$. In figure 2 we show the functions χ^2 of the one-parameter fits for each of the WCs. We also show in dashed lines the results obtained from the fits to the 2018 HFLAV average, to emphasize the change in the structure and values of the WCs needed with the new data. Horizontal lines showing the values of the 1- to 4σ ranges have been computed taking the best model (vector operators) giving $\chi^2_{\rm min} = 9.00$ as reference.

In figure 3 we show the contour plots that are obtained from each of the six two-dimensional fits to the 2019 HFLAV averages of R_D and R_{D^*}. In the appendix, table 7, we provide the correlation matrices for the fits to two WCs. We also show with empty red contours the results of the fits to the 2018 HFLAV averages. Black empty contours represent the 2σ upper limits that can be set by analyzing the tails of $pp \to \tau X$+MET at the LHC (solid line) and by estimating the projected sensitivity at the HL-LHC (dashed line) [83].

JHEP12(2019)065

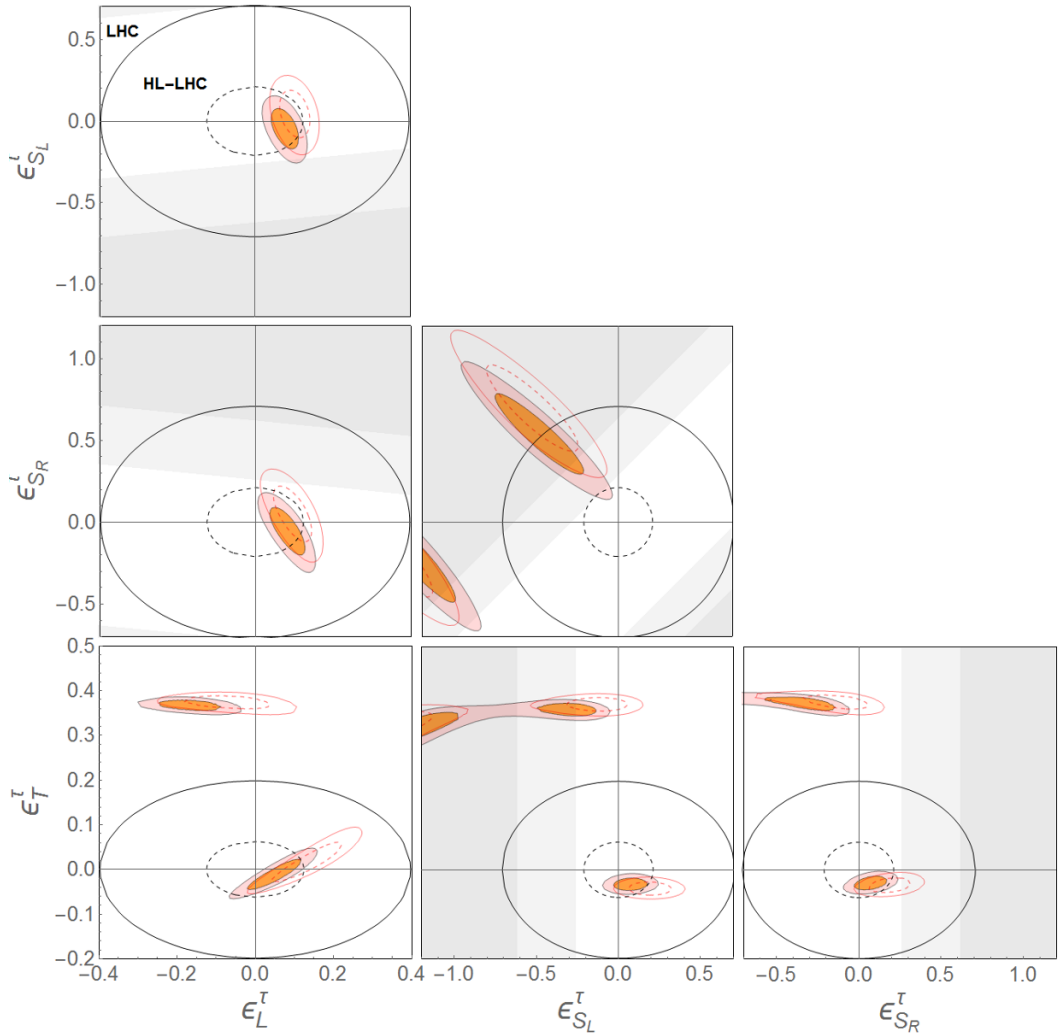

Figure 3. Constraints from the fits to R_D and R_{D^*} with two WCs active at a time (setting the others to 0) and evaluated at the renormalization scale $\mu = m_b$. Solid ellipses (empty red ellipses) represent 1σ and 2σ allowed regions from the fits to all the data (2018 HFLAV average). The empty black solid (dashed) ellipses indicate the 2σ upper bounds from the LHC data (HL-LHC projections) on $pp \to \tau_h X$+MET. Regions in gray and light gray represent 30% and 10% exclusion limits from $\mathrm{Br}(B_c \to \tau\nu)$, respectively.

Adding the new Belle data in the fit results in regions which are slightly closer to the SM, although all NP scenarios still describe the data better with a significance of 3.03σ. As expected, constraints from $\mathrm{Br}(B_c \to \tau\nu)$ play an important role in excluding regions of the parameter space of the scalar models. For instance, in case of the pure scalar fit, with $(\epsilon^{\tau}_{S_L},\ \epsilon^{\tau}_{S_R})$, the 1σ region is almost excluded by the softer limit based on the B_c lifetime. Even the 2σ region is also excluded if the more aggressive limit of 10% on $\mathrm{Br}(B_c \to \tau\nu)$ is used. Constraints in the $(\epsilon^{\tau}_{S_L},\ \epsilon^{\tau}_{T})$ plane are interesting for UV completions involving S_1 and R_2 leptoquarks. In this scenario, data favors the parameter space in which the two WCs have the opposite sign, like the contribution of the S_1 and unlike the one of

JHEP12(2019)065

the R_2, cf. eqs. (2.7) and eq. (2.9). A fit with the scalar-tensor contribution produced by the S_1 leptoquark (evaluated at $\mu = 1\,\text{TeV}$) gives a fit with a p-value 0.15 that is considerably better than for the SM. However, this scenario performs worse than those with pure left-handed or tensor operators. Constraints in the $(\epsilon_L^\tau,\ \epsilon_{S_R}^\tau)$ plane are interesting for UV completions of the U_1 leptoquark involving left- and right-handed currents to the fermions [37, 42, 47, 48].

The LHC data also probes the parameter space of the preferred regions in the different scenarios. As already anticipated in [83], scenarios involving large quadratic contributions of the tensor operator are excluded by more than 2σ. Furthermore, the current LHC exclusion region independently covers a large portion of the 1σ ellipse in the pure scalar scenario and all the parameter space of the 2σ region will be probed by the HL-LHC. In fact, with the high-luminosity data set we should be able to probe all the interesting regions in all the scenarios, although less deeply than for the results of the fits to the 2018 HFLAV average.

A potential caveat concerning the interpretation of these LHC bounds is that their validity relies on the assumption that the NP scale is significantly larger than the partonic energies probing the effective interaction in the $pp \to \tau\nu$ collisions at the LHC. In ref. [83] this was studied by assessing the sensitivity to NP of the distribution in the tau transverse-mass, m_T, of the $pp \to \tau_h X$+MET analyses [121, 122]. Most of the sensitivity of the LHC stems from $m_T \lesssim 2\,\text{TeV}$ and, for mediator masses above this mark, the EFT provides a faithful description of the NP signal. By taking the central values of the one-parameter fits shown in table 3, and assuming $\mathcal{O}(1)$ couplings in eqs. (2.5), (2.7), (2.9) and (2.11) we find that the masses of the putative new mediators are $m_{S_1} \simeq 2.3\,\text{TeV}$, $m_{U_1} \simeq 3.3\,\text{TeV}$ for left-handed current couplings and approximately a factor two lighter for right-handed current couplings, cf. $m_{W'} \simeq 1.4\,\text{TeV}$. For the tensor scenario, $m_{S_1} \simeq m_{R_2} \simeq 2.3\,\text{TeV}$. Therefore, in the comparison with the LHC bounds shown figure 3 we are implicitly assuming that the mediators are in this regime of couplings and masses.

Extending the comparison to the right-handed currents, the value $\tilde{\epsilon}_R^\tau = 0.38(6)$ obtained in the fit would still be challenged by the bound $|\tilde{\epsilon}_R^\tau| \leq 0.32$ at 2σ resulting from the collider analysis in the EFT. Turning to explicit UV completions in the range of masses below 2 TeV, LHC bounds are stronger than the EFT counterpart for the W' but weaker for the leptoquarks [83].[3]

Finally, in our fits we have assumed real WCs, but is clear from section 2.2 that these are generally complex. The imaginary part of WCs does not interfere with the leading, SM contribution. Hence it is expected that fits with purely imaginary WCs are susceptible to bounds from, eg, the rate $B_c \to \tau\nu$. This is particularly the case for scalar WCs, that require large magnitude of WCs to account for $R_{D^{(*)}}$. For example, in the left panel of figure 4 we show the fit of the complex WC ϵ_{S_L} with best fit value located at $\epsilon_{S_L} = -0.88 \pm 0.74\ i$ and where the 2σ C.L. region is excluded by the B_c lifetime and LHC constraints. However, in some cases allowing a complex phase may improve a WC

[3]For a reanalysis of the impact of the 2019 Belle data in the collider bounds using the monotau searches in the models addressing the $R_{D^{(*)}}$ anomalies see [123].

JHEP12(2019)065

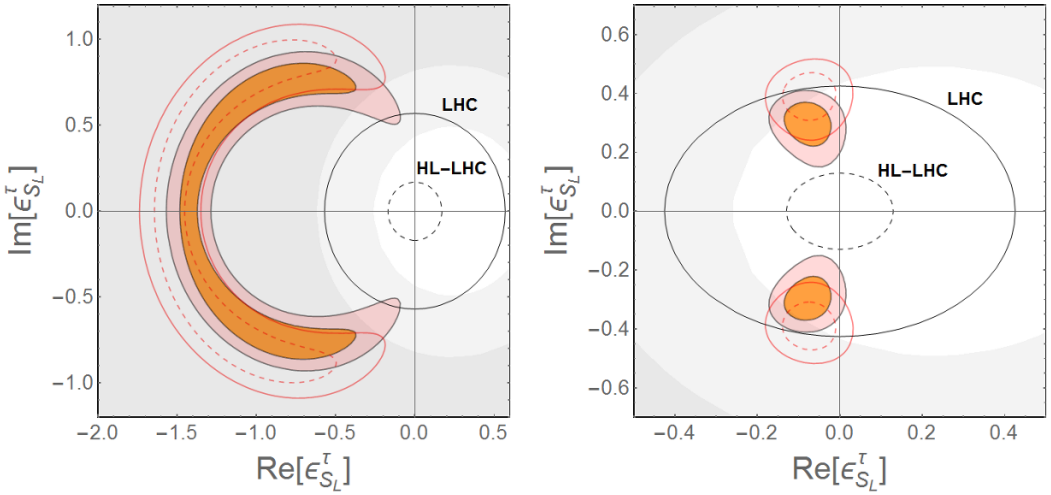

Figure 4. Constraints from the fits to R_D and R_{D^*} on the complex $\epsilon^\tau_{S_L}$ plane evaluated at the renormalization scale $\mu = m_b$: *Left:* all WCs other than $\epsilon^\tau_{S_L}$ are set to 0; *Right:* the condition $\epsilon^\tau_{S_L} = 4\epsilon^\tau_T$ is imposed at the matching scale $\mu = M_{R_2}$ =1 TeV, as in the R_2-mediator model, and all WCs other than $\epsilon^\tau_{S_L}$ and ϵ^τ_T are set to 0. Solid regions (empty red regions) represent 1σ and 2σ allowed regions from the fits to the 2019 (2018) HFLAV average of $R_{D^{(*)}}$ data. The empty black solid (dashed) ellipses indicate the 2σ upper bounds from the LHC data (HL-LHC projections) on $pp \to \tau_h X$+MET. Regions in gray and light gray represent 30% and 10% exclusion limits from $\mathrm{Br}(B_c \to \tau\nu)$, respectively.

	Best fit	$\chi^2_{\rm min}$	p-value	$\mathrm{Pull}_{\rm SM}$	1σ range
ϵ^τ_L	0.07	14.56	0.20	3.46	$(0.05, 0.09)$
ϵ^τ_T	-0.03	15.70	0.15	3.29	$(-0.04, -0.02)$
$\epsilon^\tau_{S_L}$	0.08	25.23	8.44×10^{-3}	1.14	$(0.01, 0.14)$
$\epsilon^\tau_{S_R}$	0.14	21.24	3.10×10^{-2}	2.30	$(0.08, 0.20)$
$(\epsilon^\tau_{S_L}, \epsilon^\tau_T)$	$(0.07, -0.03)$	14.75	0.14	3.00	$\epsilon^\tau_{S_L} \in (0.00, 0.13)$ $\epsilon^\tau_T \in (-0.04, -0.02)$
$(\epsilon^\tau_{S_L}, \epsilon^\tau_{S_R})$	$(-0.51, 0.56)$	12.14	0.28	3.37	$\epsilon^\tau_{S_L} \in (-0.69, -0.34)$ $\epsilon^\tau_{S_R} \in (0.41, 0.73)$
$(\epsilon^\tau_{S_R}, \epsilon^\tau_T)$	$(0.08, -0.03)$	14.38	0.16	3.05	$\epsilon^\tau_{S_R} \in (0.01, 0.14)$ $\epsilon^\tau_T \in (-0.04, -0.02)$
$(\epsilon^\tau_L, \epsilon^\tau_T)$	$(0.05, -0.01)$	14.32	0.16	3.06	$\epsilon^\tau_L \in (0.01, 0.10)$ $\epsilon^\tau_T \in (-0.03, 0.01)$
$(\epsilon^\tau_L, \epsilon^\tau_{S_L})$	$(0.08, -0.06)$	14.09	0.17	3.09	$\epsilon^\tau_L \in (0.06, 0.10)$ $\epsilon^\tau_{S_L} \in (-0.14, 0.03)$
$(\epsilon^\tau_L, \epsilon^\tau_{S_R})$	$(0.08, -0.05)$	14.33	0.16	3.06	$\epsilon^\tau_L \in (0.05, 0.11)$ $\epsilon^\tau_{S_R} \in (-0.14, 0.05)$

Table 4. Best fit values, $\chi^2_{\rm min}$, p-value, pull and 1σ confidence intervals of the WCs in the fits to all the data in R_D, R_{D^*}, $R_{J/\psi}$, $P^{D^*}_\tau$ and $F^{D^*}_L$. We perform fits to one or two WCs at a time with the understanding that the others are set to 0. For the cases of two WC fits, to take into account correlation between the two WCs, the 1σ interval of each WC is obtained by profiling over the other WC.

fit. An interesting example is that of the combination $\epsilon^\tau_{S_L} = 4\epsilon^\tau_T$ that is the case of the R_2 leptoquark mediator, eq. (2.9); the right panel of figure 4 shows the constraints on the complex $\epsilon^\tau_{S_L}(\mu = m_b)$ plane, with best fit point at $\epsilon_{S_L} = -0.08 \pm 0.30\ i$, and having imposed the condition $\epsilon^\tau_{S_L} = 4\epsilon^\tau_T$ at the matching scale $\mu = M_{R_2} = 1$ TeV.[4]

[4]Complex coefficients for a model based on R_2 were considered in ref. [43].

JHEP12(2019)065

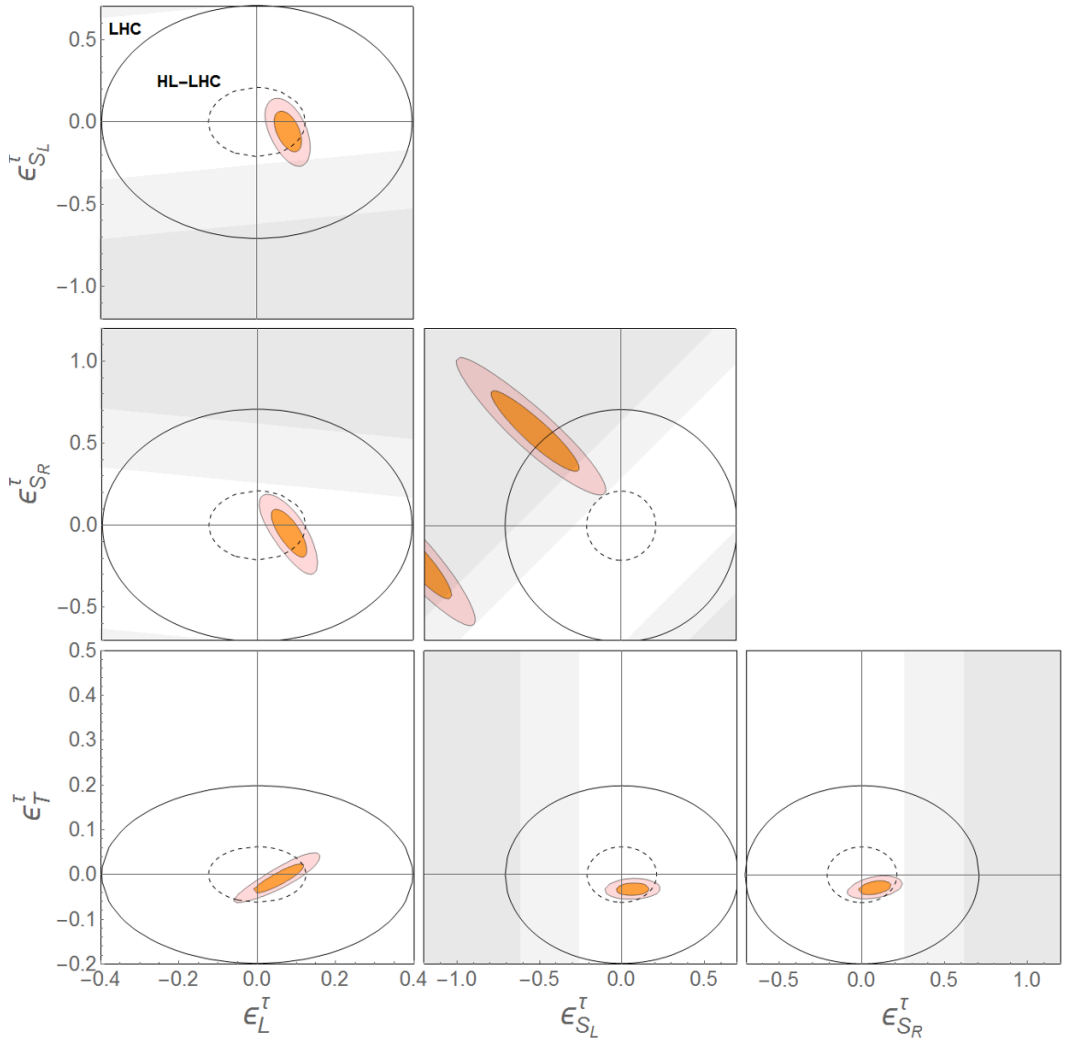

Figure 5. Constraints in the WCs planes from the fits to all the data in R_D and R_{D^*}, and to $R_{J/\psi}$, $P_\tau^{D^*}$ and $F_L^{D^*}$ setting two WCs to zero. The solid ellipses represent 1σ and 2σ allowed regions while the empty black solid (dashed) ellipses indicate the 2σ upper bounds from the LHC data (HL-LHC projections) on $pp \to \tau_h X$+MET. Regions in gray and light gray represent 30% and 10% exclusion limits from $\mathrm{Br}(B_c \to \tau\nu)$, respectively.

3.2 Fits to R_D, R_{D^*}, $R_{J/\psi}$, $P_\tau^{D^*}$ and $F_L^{D^*}$ data

In this section, we perform a global fit of ϵ_L^τ, ϵ_T^τ, $\epsilon_{S_L}^\tau$ and $\epsilon_{S_R}^\tau$ to all the data including R_D and R_{D^*}, $R_{J/\psi}$, $P_\tau^{D^*}$ and $F_L^{D^*}$. We implement the LHC monotau constraints by demanding that the WCs are within the corresponding 2σ bounds, i.e., we take $|\epsilon_L^\tau| \leq 0.32$, $|\epsilon_T^\tau| \leq 0.16$, $|\epsilon_{S_L}^\tau| \leq 0.57$ and $|\epsilon_{S_R}^\tau| \leq 0.57$. In addition, we impose the constraint from the B_c lifetime by requiring that $\mathrm{Br}(B_c \to \tau\nu) \leq 30\%$. One obtains a $\chi^2_{\mathrm{min,SM}} = 26.53$ with 12 degrees of freedom (d.o.f) if all the WCs are set to 0, corresponding to a p-value of 9.02×10^{-3}. The

JHEP12(2019)065

	Best fit	1σ range	2σ range	3σ range
ϵ_L^τ	0.16	$(-0.04, 0.36)$	$(-0.41, 0.42)$	$(-0.45, 0.47)$
ϵ_T^τ	0.05	$(-0.04, 0.14)$	$(-0.14, 0.18)$	$(-0.15, 0.23)$
$\epsilon_{S_L}^\tau$	-0.33	$(-0.54, -0.12)$	$(-1.07, 0.57)$	$(-1.11, 0.76)$
$\epsilon_{S_R}^\tau$	0.14	$(-0.08, 0.36)$	$(-1.27, 0.57)$	$(-1.34, 0.62)$

Table 5. Different confidence-level intervals of the WCs in the fits to all the data in R_D, R_{D^*}, $R_{J/\psi}$, $P_\tau^{D^*}$ and $F_L^{D^*}$, obtained from the profile χ^2 where the rest of WCs are minimized within the 2σ LHC mono-tau bound. We have also applied the 30% bound on $\mathrm{Br}(B_c \to \tau\nu)$.

resulting WCs from the fit are,

$$\begin{pmatrix} \epsilon_L^\tau \\ \epsilon_T^\tau \\ \epsilon_{S_L}^\tau \\ \epsilon_{S_R}^\tau \end{pmatrix} = \begin{pmatrix} 0.16 \pm 0.20 \\ 0.05 \pm 0.09 \\ -0.33 \pm 0.21 \\ 0.14 \pm 0.22 \end{pmatrix}, \tag{3.1}$$

with the correlation matrix,

$$\rho = \begin{pmatrix} 1.000 & 0.816 & 0.913 & -0.915 \\ & 1.000 & 0.951 & -0.920 \\ & & 1.000 & -0.986 \\ & & & 1.000 \end{pmatrix}, \tag{3.2}$$

and where $\chi^2_{\rm min} = 12.80$ for 8 d.o.f., corresponding to a p-value of 0.12 and a $\mathrm{Pull}_{\rm SM} = 2.64$. This provides an approximation of the $\chi^2_{\rm min}$ in the immediate vicinity of the minimum that is closest to the SM, although it is not appropriate to obtain realistic confidence-level regions. For instance, the 1σ intervals may seem to violate the LHC bounds described above.

In order to investigate this in more detail we perform, first, fits of two WCs to R_D and R_{D^*}, $R_{J/\psi}$, $P_\tau^{D^*}$ and $F_L^{D^*}$ setting the others to 0. This allows one to compare to the results of the two-parameters fits to R_D and R_{D^*} presented in section 3.1. The corresponding six possible combinations of two WCs fits are shown in figure 5 and the results of the fits are shown in table 4. In the appendix, table 8, we provide the correlation matrices for these fits. As compared with figure 3, one notes that although not precise, the data $R_{J/\psi}$, $P_\tau^{D^*}$ and $F_L^{D^*}$ is sensitive enough to exclude the same regions allowed at 2σ by the fit to $R_{D^{(*)}}$ independently excluded by the LHC monotau signature or $B_c \to \tau\nu$ (see also ref. [124]). However, for the favored regions of the fits closer to the SM the addition of the current data on these observables has a small impact.

Finally, in order to obtain realistic confidence-level regions with the four active WCs we obtain profile likelihoods functions depending on one or two WCs at a time. The monotau LHC constraints and the B_c lifetime bound are implicitly imposed when profiling over the other "nuisance" WCs in each case. In figure 6, we show the results of the fits as constraints in the six two-WCs plots. In table 5 we show the final 1σ, 2σ and 3σ confidence-level intervals for the WCs. The 1σ intervals are consistent with those obtained from the fit in eq. (3.1), while the 2σ and 3σ intervals differ from those obtained using the gaussian approximation of the χ^2.

JHEP12(2019)065

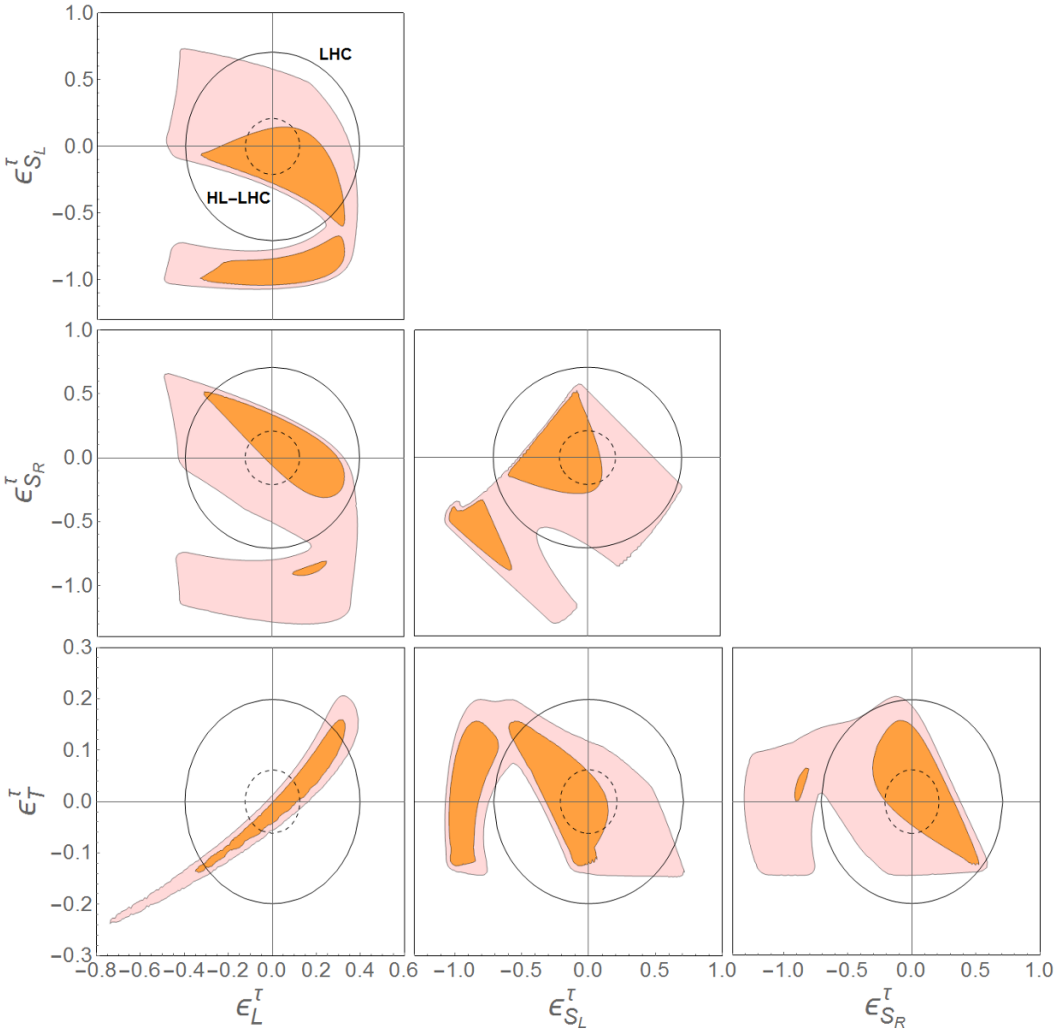

Figure 6. Constraints in the WCs planes from the fits to all the data in R_D, R_{D^*}, $R_{J/\psi}$, $P_\tau^{D^*}$ and $F_L^{D^*}$ profiling over the other WCs. The solid ellipses represent 1σ and 2σ allowed regions while the empty black solid (dashed) ellipses indicate the 2σ upper bounds from the LHC data (HL-LHC projections) on $pp \to \tau_h X + \text{MET}$. Note that we have considered the 30% bound on $\text{Br}(B_c \to \tau\nu)$.

3.3 The sensitivity of observables to New Physics

As shown above, different NP scenarios currently give a good description of the data, so the natural question is which other observables, beyond R_D and R_{D^*}, allow one to discriminate among them. Only total rates are sensitive to the effects from the vector operators as their effects cancel in normalized observables. On the other hand, scalar and tensor operators change the kinematic distributions of the decays and show up in observables such as tau and recoiling-hadron polarizations (if the latter carries spin), q^2-distribution of the rate or angular analyses.

JHEP12(2019)065

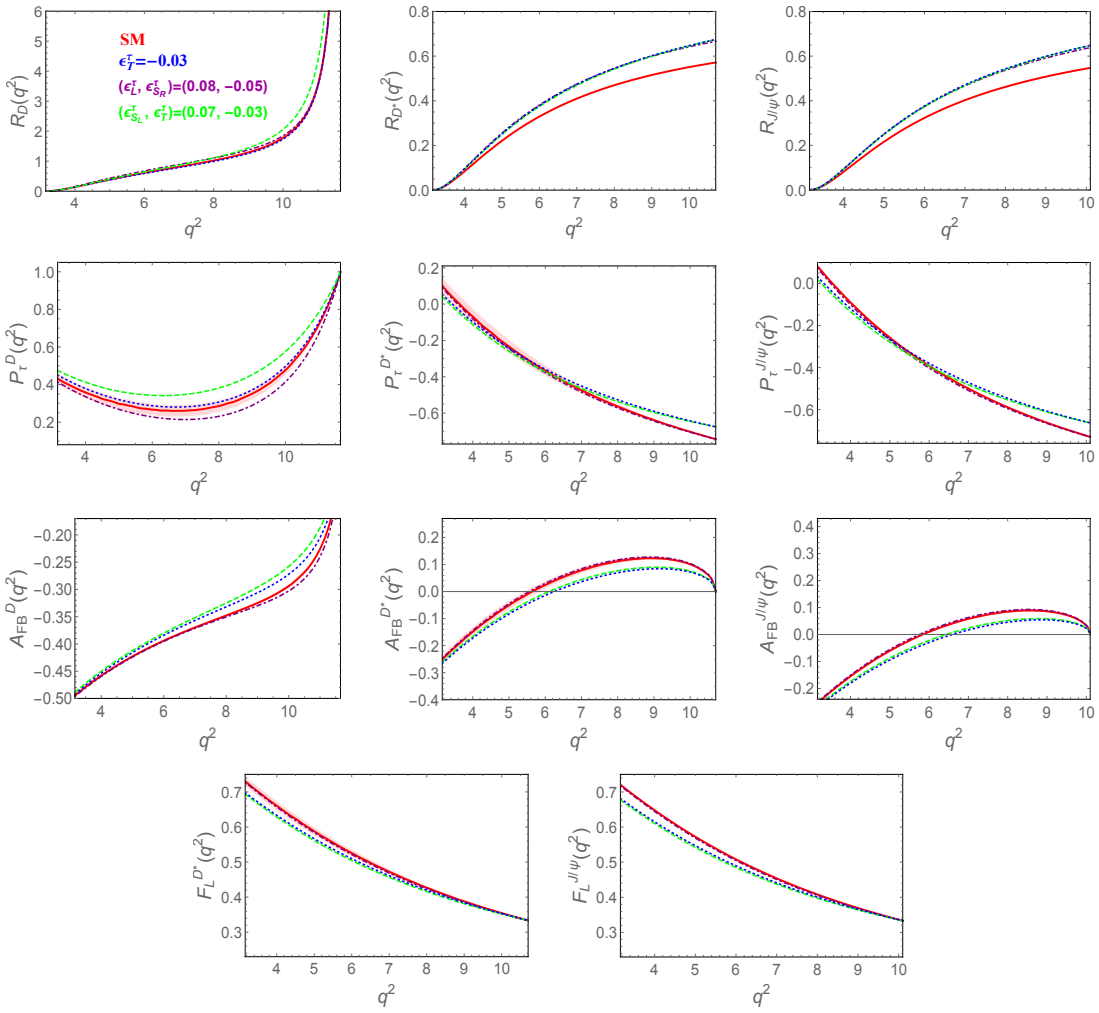

Figure 7. Dependence of all the observables on q^2 in the SM (red-solid lines) and the NP scenarios $\epsilon_T^\tau = -0.03$ (blue dotted lines), $(\epsilon_{S_L}^\tau,\ \epsilon_T^\tau) = (0.07, -0.03)$ (green dashed lines) and $(\epsilon_L^\tau,\ \epsilon_{S_R}^\tau) = (0.08, -0.05)$ (purple dot-dashed lines). Shaded area around SM curves represent the uncertainties of the SM predictions.

In figure 7, we study the q^2 spectra of $R_{D^{(*)}}$ and of a selection of polarization and angular observables[5] showing their sensitivity to NP. We select scenarios that can be motivated by UV completions such as those involving scalar-tensor or vector-scalar combinations of operators, and we also study the tensor scenario. The values of the WCs are fixed to the results of the fits to the $R_{D^{(*)}}$ data, i.e, $\epsilon_T^\tau = -0.03$, $(\epsilon_{S_L}^\tau,\ \epsilon_T^\tau) = (0.07, -0.03)$, $(\epsilon_L^\tau,\ \epsilon_{S_R}^\tau) = (0.08, -0.05)$. In table 6 we show the results of these observables integrated over the whole kinematic region for the SM and the different NP scenarios considered. In-

[5]All of them have been defined in section 1, except the tauonic forward-backward asymmetry,

$$A_{FB} = \frac{\int_0^1 \frac{d\Gamma}{d\cos\theta} d\cos\theta - \int_{-1}^0 \frac{d\Gamma}{d\cos\theta} d\cos\theta}{\int_{-1}^1 \frac{d\Gamma}{d\cos\theta} d\cos\theta}, \tag{3.3}$$

which is independent of overall normalization [125].

JHEP12(2019)065

Observables	SM	$\epsilon_T^\tau = -0.03$	$(\epsilon_{S_L}^\tau,\ \epsilon_T^\tau)$ $= (0.07, -0.03)$	$(\epsilon_L^\tau,\ \epsilon_{S_R}^\tau)$ $= (0.08, -0.05)$	$(\epsilon_L^\tau, \epsilon_T^\tau, \epsilon_{S_L}^\tau, \epsilon_{S_R}^\tau)$ $= (0.16, 0.05, -0.33, 0.14)$
R_D	$0.312^{+0.019}_{-0.018}$	$0.303^{+0.019}_{-0.018}$	$0.340^{+0.023}_{-0.021}$	$0.339^{+0.020}_{-0.018}$	$0.343^{+0.017}_{-0.016}$
P_τ^D	$0.338^{+0.033}_{-0.034}$	$0.358^{+0.033}_{-0.034}$	$0.427^{+0.032}_{-0.032}$	$0.288^{+0.034}_{-0.034}$	$0.117^{+0.033}_{-0.033}$
A_{FB}^D	$-0.358^{+0.003}_{-0.003}$	$-0.344^{+0.004}_{-0.003}$	$-0.334^{+0.005}_{-0.004}$	$-0.363^{+0.002}_{-0.002}$	$-0.383^{+0.002}_{-0.001}$
R_{D^*}	$0.253^{+0.004}_{-0.004}$	$0.293^{+0.004}_{-0.004}$	$0.291^{+0.004}_{-0.003}$	$0.293^{+0.004}_{-0.004}$	$0.297^{+0.009}_{-0.008}$
$P_\tau^{D^*}$	$-0.505^{+0.024}_{-0.022}$	$-0.477^{+0.020}_{-0.019}$	$-0.487^{+0.019}_{-0.017}$	$-0.513^{+0.023}_{-0.021}$	$-0.430^{+0.042}_{-0.041}$
$A_{FB}^{D^*}$	$0.068^{+0.013}_{-0.013}$	$0.030^{+0.012}_{-0.012}$	$0.038^{+0.012}_{-0.012}$	$0.073^{+0.013}_{-0.013}$	$0.083^{+0.017}_{-0.016}$
$F_L^{D^*}$	$0.455^{+0.009}_{-0.008}$	$0.444^{+0.008}_{-0.007}$	$0.440^{+0.007}_{-0.007}$	$0.452^{+0.008}_{-0.008}$	$0.497^{+0.015}_{-0.014}$
$R_{J/\psi}$	$0.248^{+0.003}_{-0.003}$	$0.291^{+0.004}_{-0.004}$	$0.289^{+0.004}_{-0.004}$	$0.288^{+0.004}_{-0.004}$	$0.284^{+0.003}_{-0.003}$
$P_\tau^{J/\psi}$	$-0.512^{+0.011}_{-0.010}$	$-0.481^{+0.009}_{-0.008}$	$-0.490^{+0.008}_{-0.008}$	$-0.519^{+0.010}_{-0.010}$	$-0.453^{+0.020}_{-0.019}$
$A_{FB}^{J/\psi}$	$0.042^{+0.006}_{-0.006}$	$0.007^{+0.006}_{-0.006}$	$0.013^{+0.006}_{-0.006}$	$0.046^{+0.006}_{-0.006}$	$0.061^{+0.007}_{-0.007}$
$F_L^{J/\psi}$	$0.446^{+0.003}_{-0.003}$	$0.434^{+0.003}_{-0.003}$	$0.430^{+0.002}_{-0.002}$	$0.443^{+0.003}_{-0.003}$	$0.490^{+0.005}_{-0.005}$

Table 6. Predictions in the SM and different NP scenarios for binned observables integrating over the whole kinematic regions.

terestingly, none of the preferred scenarios with up to two WCs can satisfactorily describe the Belle measurement of $F_L^{D^*}$ along with the experimental enhancements reported in R_D and R_{D^*}.

From the plots in figure 7 and predictions in table 6, one concludes that a clear pattern emerges in these observables for the different NP scenarios currently favored by the data, although high precision measurements will be required to discriminate among them. The most sensitive ones for this purpose turn out to be the tau polarization and forward-backward asymmetry of the $B \to D\tau\nu$ decay mode. Interestingly, with the 50 ab^{-1} expected to be collected by Belle II a relative statistical uncertainty better than $\sim 10\%$ has been estimated for these observables integrated over the whole q^2 region [125].

4 Summary and outlook

In this work, we have studied in detail the status of the new-physics interpretations of the $b \to c\tau\nu$ anomalies after the addition of the Belle measurements of $R_{D^{(*)}}$ using the semileptonic tag and $F_L^{D^*}$ to the data set. We perform two types of fits: first, we fit with one and two parameters (Wilson coefficients) to the 2019 HFLAV average of R_D and R_D^* with particular attention to the evolution of the preferred scenarios with the new data and to the consistency with the upper bounds that can be derived from the lifetime of the B_c meson and the $pp \to \tau_h X$+MET signature at the LHC. The main conclusion is that NP interpretations driven by left-handed currents and tensor operators are favored by the data with a significance of $\sim 3.5\sigma$ with respect to the SM hypothesis. Solutions based on pure right-handed currents remain disfavored by the LHC data while scenarios with that only have scalar contributions are in conflict with both, the LHC and the B_c-meson experimental inputs. In fact, the LHC upper bounds currently exclude large regions of

JHEP12(2019)065

the parameter space allowed by the $R_{D^{(*)}}$ data, and in the high-luminosity phase it should start probing all the interesting regions.

We also perform a second global fit of all the NP operators with (left-handed neutrinos) to the $R_{D^{(*)}}$ data, $R_{J/\Psi}$, $F_L^{D^*}$ and $P_\tau^{D^*}$. The main effect of the added observables, in particular of $F_L^{D^*}$, is to exclude the regions involving large values of the WCs, in complementarity with the upper LHC bounds. Otherwise, the favored regions by the global fits are equivalent to the ones resulting from the fit to $R_{D^{(*)}}$.

A caveat to our conclusions is that the LHC bounds derived from the analysis in terms of effective operators are not applicable if the mass scale of the new mediators they correspond to is lighter than $\sim 2\,\text{TeV}$. Scenarios based on S_1 and U_1 leptoquarks coupled to right-handed neutrinos remain challenged by the monotau signature at the LHC except for the mass range which is being independently probed by pair-production at the LHC. A S_1 leptoquark producing a scalar-tensor scenario does not provide a solution as optimal as with the 2018 HFLAV average, whereas in combination with the R_2 leptoquark it can provide the optimal tensor scenario. The R_2 leptoquark alone can also explain the data successfully when the couplings take complex values and, interestingly, its detection should be at reach in the HL-LHC. Best solutions are incarnated by the S_1 and U_1 leptoquarks with pure left-handed couplings, possibly in combination with right-hand currents in the latter case.

Finally, we investigate the sensitivity of different observables to NP. We find that the tau polarization in the $B \to D\tau\nu$ decay is sensitive to the various scenarios favored by the data. Interestingly, Belle II could achieve a precision in this observable that would provide discriminating power among them.

Acknowledgments

This work is partly supported by the National Natural Science Foundation of China under Grant No. 11735003 and by the fundamental Research Funds for the Central Universities. BG was supported in part by the US Department of Energy grant No. DE-SC0009919. SJ was supported in part by U.K. STFC Consolidated Grant ST/P000819/1. JMC acknowledges support from the Spanish MINECO through the "Ramón y Cajal" program RYC-2016-20672.

Note added: while this paper was being finished different analyses of the new data set of $R_{D^{(*)}}$ have been reported [120, 126, 127].

A Uncertainties and correlations of the two-dimensional fits

In tables 7 and 8 we provide the correlation matrices for the two-parameter fits to the 2019 HFLAV average of R_D and $R_{D^{(*)}}$, table 3, and to all the observables, table 4.

JHEP12(2019)065

	1σ uncertainty	ρ
$(\epsilon^\tau_{S_L}, \epsilon^\tau_T)$	$(\pm 0.10, \pm 0.01)$	0.079
$(\epsilon^\tau_{S_L}, \epsilon^\tau_{S_R})$	$(\pm 0.27, \pm 0.25)$	-0.925
$(\epsilon^\tau_{S_R}, \epsilon^\tau_T)$	$(\pm 0.10, \pm 0.02)$	0.275
$(\epsilon^\tau_L, \epsilon^\tau_T)$	$(\pm 0.07, \pm 0.03)$	0.896
$(\epsilon^\tau_L, \epsilon^\tau_{S_L})$	$(\pm 0.04, \pm 0.13)$	-0.496
$(\epsilon^\tau_L, \epsilon^\tau_{S_R})$	$(\pm 0.04, \pm 0.14)$	-0.733

Table 7. The 1σ uncertainty and correlation ρ for two WC fits in table 3.

	1σ uncertainty	ρ
$(\epsilon^\tau_{S_L}, \epsilon^\tau_T)$	$(\pm 0.10, \pm 0.02)$	0.070
$(\epsilon^\tau_{S_L}, \epsilon^\tau_{S_R})$	$(\pm 0.26, \pm 0.24)$	-0.921
$(\epsilon^\tau_{S_R}, \epsilon^\tau_T)$	$(\pm 0.10, \pm 0.02)$	0.256
$(\epsilon^\tau_L, \epsilon^\tau_T)$	$(\pm 0.07, \pm 0.03)$	0.891
$(\epsilon^\tau_L, \epsilon^\tau_{S_L})$	$(\pm 0.04, \pm 0.12)$	-0.487
$(\epsilon^\tau_L, \epsilon^\tau_{S_R})$	$(\pm 0.04, \pm 0.15)$	-0.732

Table 8. The 1σ uncertainty and correlation ρ for two WC fits in table 4.

References

[1] BaBar collaboration, *Evidence for an excess of $\bar{B} \to D^{(*)}\tau^-\bar{\nu}_\tau$ decays*, *Phys. Rev. Lett.* **109** (2012) 101802 [arXiv:1205.5442] [INSPIRE].

[2] BaBar collaboration, *Measurement of an excess of $\bar{B} \to D^{(*)}\tau^-\bar{\nu}_\tau$ decays and implications for charged Higgs bosons*, *Phys. Rev.* **D 88** (2013) 072012 [arXiv:1303.0571] [INSPIRE].

[3] Belle collaboration, *Measurement of the branching ratio of $\bar{B} \to D^{(*)}\tau^-\bar{\nu}_\tau$ relative to $\bar{B} \to D^{(*)}\ell^-\bar{\nu}_\ell$ decays with hadronic tagging at Belle*, *Phys. Rev.* **D 92** (2015) 072014 [arXiv:1507.03233] [INSPIRE].

[4] Belle collaboration, *Measurement of the branching ratio of $\bar{B}^0 \to D^{*+}\tau^-\bar{\nu}_\tau$ relative to $\bar{B}^0 \to D^{*+}\ell^-\bar{\nu}_\ell$ decays with a semileptonic tagging method*, *Phys. Rev.* **D 94** (2016) 072007 [arXiv:1607.07923] [INSPIRE].

[5] LHCb collaboration, *Measurement of the ratio of branching fractions $\mathcal{B}(\bar{B}^0 \to D^{*+}\tau^-\bar{\nu}_\tau)/\mathcal{B}(\bar{B}^0 \to D^{*+}\mu^-\bar{\nu}_\mu)$*, *Phys. Rev. Lett.* **115** (2015) 111803 [*Erratum ibid.* **115** (2015) 159901] [arXiv:1506.08614] [INSPIRE].

[6] Belle collaboration, *Measurement of the τ lepton polarization and $R(D^*)$ in the decay $\bar{B} \to D^*\tau^-\bar{\nu}_\tau$*, *Phys. Rev. Lett.* **118** (2017) 211801 [arXiv:1612.00529] [INSPIRE].

[7] Belle collaboration, *Measurement of the τ lepton polarization and $R(D^*)$ in the decay $\bar{B} \to D^*\tau^-\bar{\nu}_\tau$ with one-prong hadronic τ decays at Belle*, *Phys. Rev.* **D 97** (2018) 012004 [arXiv:1709.00129] [INSPIRE].

[8] LHCb collaboration, *Measurement of the ratio of the $B^0 \to D^{*-}\tau^+\nu_\tau$ and $B^0 \to D^{*-}\mu^+\nu_\mu$ branching fractions using three-prong τ-lepton decays*, *Phys. Rev. Lett.* **120** (2018) 171802 [arXiv:1708.08856] [INSPIRE].

JHEP12(2019)065

[9] LHCb collaboration, *Test of lepton flavor universality by the measurement of the $B^0 \to D^{*-}\tau^+\nu_\tau$ branching fraction using three-prong τ decays*, *Phys. Rev.* **D 97** (2018) 072013 [arXiv:1711.02505] [INSPIRE].

[10] LHCb collaboration, *Measurement of the ratio of branching fractions $\mathcal{B}(B_c^+ \to J/\psi\tau^+\nu_\tau)/\mathcal{B}(B_c^+ \to J/\psi\mu^+\nu_\mu)$*, *Phys. Rev. Lett.* **120** (2018) 121801 [arXiv:1711.05623] [INSPIRE].

[11] S. Aoki et al., *Review of lattice results concerning low-energy particle physics*, *Eur. Phys. J.* **C 77** (2017) 112 [arXiv:1607.00299] [INSPIRE].

[12] E. Megias, M. Quirós and L. Salas, *Lepton-flavor universality violation in R_K and $R_{D^{(*)}}$ from warped space*, *JHEP* **07** (2017) 102 [arXiv:1703.06019] [INSPIRE].

[13] X.-G. He and G. Valencia, *Lepton universality violation and right-handed currents in $b \to c\tau\nu$*, *Phys. Lett.* **B 779** (2018) 52 [arXiv:1711.09525] [INSPIRE].

[14] S. Matsuzaki, K. Nishiwaki and R. Watanabe, *Phenomenology of flavorful composite vector bosons in light of B anomalies*, *JHEP* **08** (2017) 145 [arXiv:1706.01463] [INSPIRE].

[15] K.S. Babu, B. Dutta and R.N. Mohapatra, *A theory of $R(D^*, D)$ anomaly with right-handed currents*, *JHEP* **01** (2019) 168 [arXiv:1811.04496] [INSPIRE].

[16] A. Greljo, D.J. Robinson, B. Shakya and J. Zupan, *$R(D^{(*)})$ from W' and right-handed neutrinos*, *JHEP* **09** (2018) 169 [arXiv:1804.04642] [INSPIRE].

[17] P. Asadi, M.R. Buckley and D. Shih, *It's all right(-handed neutrinos): a new W' model for the $R_{D^{(*)}}$ anomaly*, *JHEP* **09** (2018) 010 [arXiv:1804.04135] [INSPIRE].

[18] M. Tanaka, *Charged Higgs effects on exclusive semitauonic B decays*, *Z. Phys.* **C 67** (1995) 321 [hep-ph/9411405] [INSPIRE].

[19] A. Celis, M. Jung, X.-Q. Li and A. Pich, *Sensitivity to charged scalars in $B \to D^{(*)}\tau\nu_\tau$ and $B \to \tau\nu_\tau$ decays*, *JHEP* **01** (2013) 054 [arXiv:1210.8443] [INSPIRE].

[20] A. Celis, M. Jung, X.-Q. Li and A. Pich, *Scalar contributions to $b \to c(u)\tau\nu$ transitions*, *Phys. Lett.* **B 771** (2017) 168 [arXiv:1612.07757] [INSPIRE].

[21] S. Iguro and K. Tobe, *$R(D^{(*)})$ in a general two Higgs doublet model*, *Nucl. Phys.* **B 925** (2017) 560 [arXiv:1708.06176] [INSPIRE].

[22] S. Fraser et al., *Towards a viable scalar interpretation of $R_{D^{(*)}}$*, *Phys. Rev.* **D 98** (2018) 035016 [arXiv:1805.08189] [INSPIRE].

[23] R. Martinez, C.F. Sierra and G. Valencia, *Beyond $\mathcal{R}(D^{(*)})$ with the general type-III 2HDM for $b \to c\tau\nu$*, *Phys. Rev.* **D 98** (2018) 115012 [arXiv:1805.04098] [INSPIRE].

[24] Y. Sakaki, M. Tanaka, A. Tayduganov and R. Watanabe, *Testing leptoquark models in $\bar{B} \to D^{(*)}\tau\bar{\nu}$*, *Phys. Rev.* **D 88** (2013) 094012 [arXiv:1309.0301] [INSPIRE].

[25] R. Alonso, B. Grinstein and J. Martin Camalich, *Lepton universality violation and lepton flavor conservation in B-meson decays*, *JHEP* **10** (2015) 184 [arXiv:1505.05164] [INSPIRE].

[26] R. Barbieri, G. Isidori, A. Pattori and F. Senia, *Anomalies in B-decays and $U(2)$ flavour symmetry*, *Eur. Phys. J.* **C 76** (2016) 67 [arXiv:1512.01560] [INSPIRE].

[27] M. Freytsis, Z. Ligeti and J.T. Ruderman, *Flavor models for $\bar{B} \to D^{(*)}\tau\bar{\nu}$*, *Phys. Rev.* **D 92** (2015) 054018 [arXiv:1506.08896] [INSPIRE].

[28] S. Fajfer and N. Košnik, *Vector leptoquark resolution of R_K and $R_{D^{(*)}}$ puzzles*, *Phys. Lett.* **B 755** (2016) 270 [arXiv:1511.06024] [INSPIRE].

JHEP12(2019)065

[29] M. Bauer and M. Neubert, *Minimal leptoquark explanation for the $R_{D^{(*)}}$, R_K and $(g-2)_g$ anomalies*, *Phys. Rev. Lett.* **116** (2016) 141802 [arXiv:1511.01900] [INSPIRE].

[30] X.-Q. Li, Y.-D. Yang and X. Zhang, *Revisiting the one leptoquark solution to the $R(D^{(*)})$ anomalies and its phenomenological implications*, *JHEP* **08** (2016) 054 [arXiv:1605.09308] [INSPIRE].

[31] R. Barbieri, C.W. Murphy and F. Senia, *B-decay anomalies in a composite leptoquark model*, *Eur. Phys. J.* **C 77** (2017) 8 [arXiv:1611.04930] [INSPIRE].

[32] D. Bečirević, S. Fajfer, N. Košnik and O. Sumensari, *Leptoquark model to explain the B-physics anomalies, R_K and R_D*, *Phys. Rev.* **D 94** (2016) 115021 [arXiv:1608.08501] [INSPIRE].

[33] A. Crivellin, D. Müller and T. Ota, *Simultaneous explanation of $R(D^{(*)})$ and $b \to s\mu^+\mu^-$: the last scalar leptoquarks standing*, *JHEP* **09** (2017) 040 [arXiv:1703.09226] [INSPIRE].

[34] Y. Cai, J. Gargalionis, M.A. Schmidt and R.R. Volkas, *Reconsidering the One Leptoquark solution: flavor anomalies and neutrino mass*, *JHEP* **10** (2017) 047 [arXiv:1704.05849] [INSPIRE].

[35] N. Assad, B. Fornal and B. Grinstein, *Baryon number and lepton universality violation in leptoquark and diquark models*, *Phys. Lett.* **B 777** (2018) 324 [arXiv:1708.06350] [INSPIRE].

[36] L. Di Luzio, A. Greljo and M. Nardecchia, *Gauge leptoquark as the origin of B-physics anomalies*, *Phys. Rev.* **D 96** (2017) 115011 [arXiv:1708.08450] [INSPIRE].

[37] M. Bordone, C. Cornella, J. Fuentes-Martin and G. Isidori, *A three-site gauge model for flavor hierarchies and flavor anomalies*, *Phys. Lett.* **B 779** (2018) 317 [arXiv:1712.01368] [INSPIRE].

[38] W. Altmannshofer, P.S. Bhupal Dev and A. Soni, *$R_{D^{(*)}}$ anomaly: a possible hint for natural supersymmetry with R-parity violation*, *Phys. Rev.* **D 96** (2017) 095010 [arXiv:1704.06659] [INSPIRE].

[39] A. Monteux and A. Rajaraman, *B anomalies and Leptoquarks at the LHC: beyond the lepton-quark final state*, *Phys. Rev.* **D 98** (2018) 115032 [arXiv:1803.05962] [INSPIRE].

[40] D. Marzocca, *Addressing the B-physics anomalies in a fundamental composite Higgs model*, *JHEP* **07** (2018) 121 [arXiv:1803.10972] [INSPIRE].

[41] M. Blanke and A. Crivellin, *B meson anomalies in a Pati-Salam model within the Randall-Sundrum background*, *Phys. Rev. Lett.* **121** (2018) 011801 [arXiv:1801.07256] [INSPIRE].

[42] M. Bordone, C. Cornella, J. Fuentes-Martín and G. Isidori, *Low-energy signatures of the PS^3 model: from B-physics anomalies to LFV*, *JHEP* **10** (2018) 148 [arXiv:1805.09328] [INSPIRE].

[43] D. Bečirević et al., *Scalar leptoquarks from grand unified theories to accommodate the B-physics anomalies*, *Phys. Rev.* **D 98** (2018) 055003 [arXiv:1806.05689] [INSPIRE].

[44] A. Crivellin, C. Greub, D. Müller and F. Saturnino, *Importance of loop effects in explaining the accumulated evidence for new physics in B decays with a vector leptoquark*, *Phys. Rev. Lett.* **122** (2019) 011805 [arXiv:1807.02068] [INSPIRE].

[45] B. Fornal, S.A. Gadam and B. Grinstein, *Left-right* SU(4) *vector leptoquark model for flavor anomalies*, *Phys. Rev.* **D 99** (2019) 055025 [arXiv:1812.01603] [INSPIRE].

JHEP12(2019)065

[46] A. Angelescu, D. Bečirević, D.A. Faroughy and O. Sumensari, *Closing the window on single leptoquark solutions to the B-physics anomalies*, *JHEP* **10** (2018) 183 [arXiv:1808.08179] [INSPIRE].

[47] M.J. Baker, J. Fuentes-Martín, G. Isidori and M. König, *High-p_T signatures in vector-leptoquark models*, *Eur. Phys. J.* **C 79** (2019) 334 [arXiv:1901.10480] [INSPIRE].

[48] C. Cornella, J. Fuentes-Martin and G. Isidori, *Revisiting the vector leptoquark explanation of the B-physics anomalies*, *JHEP* **07** (2019) 168 [arXiv:1903.11517] [INSPIRE].

[49] O. Popov, M.A. Schmidt and G. White, *R_2 as a single leptoquark solution to $R_{D^{(*)}}$ and $R_{K^{(*)}}$*, *Phys. Rev.* **D 100** (2019) 035028 [arXiv:1905.06339] [INSPIRE].

[50] BELLE collaboration, *Measurement of the D^{*-} polarization in the decay $B^0 \to D^{*-}\tau^+\nu_\tau$*, talk given at the 10th *International Workshop on the CKM Unitarity Triangle (CKM 2018)*, September 17–21, Heidelberg, Germany (2018), arXiv:1903.03102 [INSPIRE].

[51] BELLE collaboration, *Measurement of $\mathcal{R}(D)$ and $\mathcal{R}(D^*)$ with a semileptonic tagging method*, arXiv:1904.08794 [INSPIRE].

[52] D. Buttazzo, A. Greljo, G. Isidori and D. Marzocca, *B-physics anomalies: a guide to combined explanations*, *JHEP* **11** (2017) 044 [arXiv:1706.07808] [INSPIRE].

[53] A.K. Alok, D. Kumar, J. Kumar, S. Kumbhakar and S.U. Sankar, *New physics solutions for R_D and R_{D^*}*, *JHEP* **09** (2018) 152 [arXiv:1710.04127] [INSPIRE].

[54] A. Azatov, D. Bardhan, D. Ghosh, F. Sgarlata and E. Venturini, *Anatomy of $b \to c\tau\nu$ anomalies*, *JHEP* **11** (2018) 187 [arXiv:1805.03209] [INSPIRE].

[55] S. Bhattacharya, S. Nandi and S. Kumar Patra, *$b \to c\tau\nu_\tau$ decays: a catalogue to compare, constrain and correlate new physics effects*, *Eur. Phys. J.* **C 79** (2019) 268 [arXiv:1805.08222] [INSPIRE].

[56] Z.-R. Huang, Y. Li, C.-D. Lu, M.A. Paracha and C. Wang, *Footprints of new physics in $b \to c\tau\nu$ transitions*, *Phys. Rev.* **D 98** (2018) 095018 [arXiv:1808.03565] [INSPIRE].

[57] P. Asadi, M.R. Buckley and D. Shih, *Asymmetry observables and the origin of $R_{D^{(*)}}$ anomalies*, *Phys. Rev.* **D 99** (2019) 035015 [arXiv:1810.06597] [INSPIRE].

[58] M. Blanke et al., *Impact of polarization observables and $B_c \to \tau\nu$ on new physics explanations of the $b \to c\tau\nu$ anomaly*, *Phys. Rev.* **D 99** (2019) 075006 [arXiv:1811.09603] [INSPIRE].

[59] R. Dutta and A. Bhol, *$B_c \to (J/\psi, \eta_c)\tau\nu$ semileptonic decays within the standard model and beyond*, *Phys. Rev.* **D 96** (2017) 076001 [arXiv:1701.08598] [INSPIRE].

[60] R. Dutta, A. Bhol and A.K. Giri, *Effective theory approach to new physics in $b \to u$ and $b \to c$ leptonic and semileptonic decays*, *Phys. Rev.* **D 88** (2013) 114023 [arXiv:1307.6653] [INSPIRE].

[61] Q.-Y. Hu, X.-Q. Li and Y.-D. Yang, *$b \to c\tau\nu$ transitions in the standard model effective field theory*, *Eur. Phys. J.* **C 79** (2019) 264 [arXiv:1810.04939] [INSPIRE].

[62] A.K. Alok, D. Kumar, S. Kumbhakar and S.U. Sankar, *D^* polarization as a probe to discriminate new physics in $\bar{B} \to D^*\tau\bar{\nu}$*, *Phys. Rev.* **D 95** (2017) 115038 [arXiv:1606.03164] [INSPIRE].

[63] A.K. Alok, D. Kumar, S. Kumbhakar and S. Uma Sankar, *Resolution of R_D/R_{D^*} puzzle*, *Phys. Lett.* **B 784** (2018) 16 [arXiv:1804.08078] [INSPIRE].

[64] M. Jung and D.M. Straub, *Constraining new physics in $b \to c\ell\nu$ transitions*, *JHEP* **01** (2019) 009 [arXiv:1801.01112] [INSPIRE].

JHEP12(2019)065

[65] HFLAV collaboration, *Averages of b-hadron, c-hadron and τ-lepton properties as of summer 2016*, *Eur. Phys. J.* **C 77** (2017) 895 [arXiv:1612.07233] [INSPIRE].

[66] W. Buchmüller and D. Wyler, *Effective Lagrangian analysis of new interactions and flavor conservation*, *Nucl. Phys.* **B 268** (1986) 621 [INSPIRE].

[67] B. Grzadkowski, M. Iskrzynski, M. Misiak and J. Rosiek, *Dimension-Six Terms in the Standard Model Lagrangian*, *JHEP* **10** (2010) 085 [arXiv:1008.4884] [INSPIRE].

[68] V. Bernard, M. Oertel, E. Passemar and J. Stern, *$K(\mu_3)^L$ decay: a stringent test of right-handed quark currents*, *Phys. Lett.* **B 638** (2006) 480 [hep-ph/0603202] [INSPIRE].

[69] V. Cirigliano, J. Jenkins and M. Gonzalez-Alonso, *Semileptonic decays of light quarks beyond the Standard Model*, *Nucl. Phys.* **B 830** (2010) 95 [arXiv:0908.1754] [INSPIRE].

[70] O. Catà and M. Jung, *Signatures of a nonstandard Higgs boson from flavor physics*, *Phys. Rev.* **D 92** (2015) 055018 [arXiv:1505.05804] [INSPIRE].

[71] M. González-Alonso, J. Martin Camalich and K. Mimouni, *Renormalization-group evolution of new physics contributions to (semi)leptonic meson decays*, *Phys. Lett.* **B 772** (2017) 777 [arXiv:1706.00410] [INSPIRE].

[72] J. Aebischer, M. Fael, C. Greub and J. Virto, *B physics beyond the standard model at one loop: complete renormalization group evolution below the electroweak scale*, *JHEP* **09** (2017) 158 [arXiv:1704.06639] [INSPIRE].

[73] E.E. Jenkins, A.V. Manohar and P. Stoffer, *Low-energy effective field theory below the electroweak scale: anomalous dimensions*, *JHEP* **01** (2018) 084 [arXiv:1711.05270] [INSPIRE].

[74] F. Feruglio, P. Paradisi and O. Sumensari, *Implications of scalar and tensor explanations of $R_{D^{(*)}}$*, *JHEP* **11** (2018) 191 [arXiv:1806.10155] [INSPIRE].

[75] A. Sirlin, *Large $m(W)$, $m(Z)$ behavior of the $O(\alpha)$ corrections to semileptonic processes mediated by W*, *Nucl. Phys.* **B 196** (1982) 83 [INSPIRE].

[76] F. Feruglio, P. Paradisi and A. Pattori, *Revisiting lepton flavor universality in B decays*, *Phys. Rev. Lett.* **118** (2017) 011801 [arXiv:1606.00524] [INSPIRE].

[77] F. Feruglio, P. Paradisi and A. Pattori, *On the importance of electroweak corrections for B anomalies*, *JHEP* **09** (2017) 061 [arXiv:1705.00929] [INSPIRE].

[78] D.J. Robinson, B. Shakya and J. Zupan, *Right-handed neutrinos and $R(D^{(*)})$*, *JHEP* **02** (2019) 119 [arXiv:1807.04753] [INSPIRE].

[79] A. Azatov et al., *Combined explanations of B-physics anomalies: the sterile neutrino solution*, *JHEP* **10** (2018) 092 [arXiv:1807.10745] [INSPIRE].

[80] W.D. Goldberger, *Semileptonic B decays as a probe of new physics*, hep-ph/9902311 [INSPIRE].

[81] R. Alonso, B. Grinstein and J. Martin Camalich, *Lifetime of B_c^- Constrains Explanations for Anomalies in $B \to D^{(*)}\tau\nu$*, *Phys. Rev. Lett.* **118** (2017) 081802 [arXiv:1611.06676] [INSPIRE].

[82] A.G. Akeroyd and C.-H. Chen, *Constraint on the branching ratio of $B_c \to \tau\bar{\nu}$ from LEP1 and consequences for $R(D^{(*)})$ anomaly*, *Phys. Rev.* **D 96** (2017) 075011 [arXiv:1708.04072] [INSPIRE].

[83] A. Greljo, J. Martin Camalich and J.D. Ruiz-Álvarez, *Mono-τ signatures at the LHC constrain explanations of B-decay anomalies*, *Phys. Rev. Lett.* **122** (2019) 131803 [arXiv:1811.07920] [INSPIRE].

JHEP12(2019)065

[84] D.A. Faroughy, A. Greljo and J.F. Kamenik, *Confronting lepton flavor universality violation in B decays with high-p_T tau lepton searches at LHC*, *Phys. Lett.* **B 764** (2017) 126 [arXiv:1609.07138] [INSPIRE].

[85] S. Iguro, Y. Omura and M. Takeuchi, *Test of the $R(D^{(*)})$ anomaly at the LHC*, *Phys. Rev.* **D 99** (2019) 075013 [arXiv:1810.05843] [INSPIRE].

[86] W. Buchmüller, R. Ruckl and D. Wyler, *Leptoquarks in lepton-quark collisions*, *Phys. Lett.* **B 191** (1987) 442 [*Erratum ibid.* **B 448** (1999) 320] [INSPIRE].

[87] I. Doršner et al., *Physics of leptoquarks in precision experiments and at particle colliders*, *Phys. Rept.* **641** (2016) 1 [arXiv:1603.04993] [INSPIRE].

[88] Particle Data Group collaboration, *Review of particle physics*, *Phys. Rev.* **D 98** (2018) 030001 [INSPIRE].

[89] G. Buchalla, A.J. Buras and M.E. Lautenbacher, *Weak decays beyond leading logarithms*, *Rev. Mod. Phys.* **68** (1996) 1125 [hep-ph/9512380] [INSPIRE].

[90] HPQCD collaboration, *$B \to Dl\nu$ form factors at nonzero recoil and extraction of $|V_{cb}|$*, *Phys. Rev.* **D 92** (2015) 054510 [*Erratum ibid.* **D 93** (2016) 119906] [arXiv:1505.03925] [INSPIRE].

[91] Fermilab Lattice, MILC collaboration, *Update of $|V_{cb}|$ from the $\bar{B} \to D^* \ell \bar{\nu}$ form factor at zero recoil with three-flavor lattice QCD*, *Phys. Rev.* **D 89** (2014) 114504 [arXiv:1403.0635] [INSPIRE].

[92] M.A. Shifman and M.B. Voloshin, *On production of d and D^* Mesons in B meson decays*, *Sov. J. Nucl. Phys.* **47** (1988) 511 [INSPIRE].

[93] N. Isgur and M.B. Wise, *Weak decays of heavy mesons in the static quark approximation*, *Phys. Lett.* **B 232** (1989) 113 [INSPIRE].

[94] N. Isgur and M.B. Wise, *Weak transition form-factors between heavy mesons*, *Phys. Lett.* **B 237** (1990) 527 [INSPIRE].

[95] A.F. Falk, H. Georgi, B. Grinstein and M.B. Wise, *Heavy meson form-factors from QCD*, *Nucl. Phys.* **B 343** (1990) 1 [INSPIRE].

[96] C.G. Boyd, B. Grinstein and R.F. Lebed, *Constraints on form-factors for exclusive semileptonic heavy to light meson decays*, *Phys. Rev. Lett.* **74** (1995) 4603 [hep-ph/9412324] [INSPIRE].

[97] C.G. Boyd, B. Grinstein and R.F. Lebed, *Model independent extraction of $|V(cb)|$ using dispersion relations*, *Phys. Lett.* **B 353** (1995) 306 [hep-ph/9504235] [INSPIRE].

[98] I. Caprini, L. Lellouch and M. Neubert, *Dispersive bounds on the shape of $\bar{B} \to D^{(*)}$ lepton anti-neutrino form-factors*, *Nucl. Phys.* **B 530** (1998) 153 [hep-ph/9712417] [INSPIRE].

[99] S. Fajfer, J.F. Kamenik and I. Nisandzic, *On the $B \to D^* \tau \bar{\nu}_\tau$ sensitivity to new physics*, *Phys. Rev.* **D 85** (2012) 094025 [arXiv:1203.2654] [INSPIRE].

[100] Heavy Flavor Averaging Group (HFAG) collaboration, *Averages of b-hadron, c-hadron and τ-lepton properties as of summer 2014*, arXiv:1412.7515 [INSPIRE].

[101] R. Alonso, A. Kobach and J. Martin Camalich, *New physics in the kinematic distributions of $\bar{B} \to D^{(*)} \tau^- (\to \ell^- \bar{\nu}_\ell \nu_\tau) \bar{\nu}_\tau$*, *Phys. Rev.* **D 94** (2016) 094021 [arXiv:1602.07671] [INSPIRE].

[102] F.U. Bernlochner, Z. Ligeti, M. Papucci and D.J. Robinson, *Combined analysis of semileptonic B decays to D and D^*: $R(D^{(*)})$, $|V_{cb}|$ and new physics*, *Phys. Rev.* **D 95** (2017) 115008 [arXiv:1703.05330] [INSPIRE].

JHEP12(2019)065

[103] D. Bigi, P. Gambino and S. Schacht, *$R(D^*)$, $|V_{cb}|$ and the heavy quark symmetry relations between form factors*, *JHEP* **11** (2017) 061 [arXiv:1707.09509] [INSPIRE].

[104] S. Jaiswal, S. Nandi and S.K. Patra, *Extraction of $|V_{cb}|$ from $B \to D^{(*)}\ell\nu_\ell$ and the standard model predictions of $R(D^{(*)})$*, *JHEP* **12** (2017) 060 [arXiv:1707.09977] [INSPIRE].

[105] W.-F. Wang, Y.-Y. Fan and Z.-J. Xiao, *Semileptonic decays $B_c \to (\eta_c, J/\Psi)l\nu$ in the perturbative QCD approach*, *Chin. Phys.* **C 37** (2013) 093102 [arXiv:1212.5903] [INSPIRE].

[106] V.V. Kiselev, *Exclusive decays and lifetime of B_c meson in QCD sum rules*, hep-ph/0211021 [INSPIRE].

[107] H.-B. Fu et al., *Longitudinal leading-twist distribution amplitude of the J/ψ meson within the background field theory*, *Phys. Rev.* **D 97** (2018) 074025 [arXiv:1801.06832] [INSPIRE].

[108] R. Zhu, Y. Ma, X.-L. Han and Z.-J. Xiao, *Relativistic corrections to the form factors of B_c into S-wave charmonium*, *Phys. Rev.* **D 95** (2017) 094012 [arXiv:1703.03875] [INSPIRE].

[109] J.-M. Shen, X.-G. Wu, H.-H. Ma and S.-Q. Wang, *QCD corrections to the B_c to charmonia semileptonic decays*, *Phys. Rev.* **D 90** (2014) 034025 [arXiv:1407.7309] [INSPIRE].

[110] W. Wang, Y.-L. Shen and C.-D. Lu, *Covariant light-front approach for $B(c)$ transition form factors*, *Phys. Rev.* **D 79** (2009) 054012 [arXiv:0811.3748] [INSPIRE].

[111] E. Hernandez, J. Nieves and J.M. Verde-Velasco, *Study of exclusive semileptonic and non-leptonic decays of B_c — in a nonrelativistic quark model*, *Phys. Rev.* **D 74** (2006) 074008 [hep-ph/0607150] [INSPIRE].

[112] D. Ebert, R.N. Faustov and V.O. Galkin, *Weak decays of the B_c meson to charmonium and D mesons in the relativistic quark model*, *Phys. Rev.* **D 68** (2003) 094020 [hep-ph/0306306] [INSPIRE].

[113] A. Lytle et al., *Semileptonic B_c decays from full lattice QCD*, PoS(BEAUTY2016)069 [arXiv:1605.05645] [INSPIRE].

[114] HPQCD collaboration, *B_c decays from highly improved staggered quarks and NRQCD*, PoS(LATTICE 2016)281 [arXiv:1611.01987] [INSPIRE].

[115] C.-T. Tran, M.A. Ivanov, J.G. Körner and P. Santorelli, *Implications of new physics in the decays $B_c \to (J/\psi, \eta_c)\tau\nu$*, *Phys. Rev.* **D 97** (2018) 054014 [arXiv:1801.06927] [INSPIRE].

[116] R. Watanabe, *New Physics effect on $B_c \to J/\psi\tau\bar{\nu}$ in relation to the $R_{D^{(*)}}$ anomaly*, *Phys. Lett.* **B 776** (2018) 5 [arXiv:1709.08644] [INSPIRE].

[117] R. Dutta, *Exploring R_D, R_{D^*} and $R_{J/\Psi}$ anomalies*, arXiv:1710.00351 [INSPIRE].

[118] T.D. Cohen, H. Lamm and R.F. Lebed, *Model-independent bounds on $R(J/\psi)$*, *JHEP* **09** (2018) 168 [arXiv:1807.02730] [INSPIRE].

[119] M. Blanke et al., *Addendum to "Impact of polarization observables and $B_c \to \tau\nu$ on new physics explanations of the $b \to c\tau\nu$ anomaly"*, *Phys. Rev.* **D 100** (2019) 035035 [arXiv:1905.08253] [INSPIRE].

[120] D. Bardhan and D. Ghosh, *B -meson charged current anomalies: the post-Moriond 2019 status*, *Phys. Rev.* **D 100** (2019) 011701 [arXiv:1904.10432] [INSPIRE].

[121] ATLAS collaboration, *Search for high-mass resonances decaying to $\tau\nu$ in pp collisions at $\sqrt{s} = 13$ TeV with the ATLAS detector*, *Phys. Rev. Lett.* **120** (2018) 161802 [arXiv:1801.06992] [INSPIRE].

[122] CMS collaboration, *Search for a W' boson decaying to a τ lepton and a neutrino in proton-proton collisions at $\sqrt{s} = 13$ TeV*, *Phys. Lett.* **B 792** (2019) 107 [arXiv:1807.11421] [INSPIRE].

JHEP12(2019)065

[123] J. Martin Camalich, *Flavored mono-tau searches at the LHC*, talk given at *Portorož 2019, Precision era in High Energy Physics*, April 16–19, Portorož, Slovenia (2019).

[124] J. Aebischer, J. Kumar, P. Stangl and D.M. Straub, *A global likelihood for precision constraints and flavour anomalies*, *Eur. Phys. J.* **C 79** (2019) 509 [arXiv:1810.07698] [INSPIRE].

[125] R. Alonso, J. Martin Camalich and S. Westhoff, *τ properties in $B \to D\tau\nu$ from visible final-state kinematics*, *Phys. Rev.* **D 95** (2017) 093006 [arXiv:1702.02773] [INSPIRE].

[126] C. Murgui, A. Peñuelas, M. Jung and A. Pich, *Global fit to $b \to c\tau\nu$ transitions*, *JHEP* **09** (2019) 103 [arXiv:1904.09311] [INSPIRE].

[127] P. Asadi and D. Shih, *Maximizing the impact of new physics in $b \to c\tau\nu$ anomalies*, arXiv:1905.03311 [INSPIRE].

JHEP12(2019)065